https://ntrs.nasa.gov/search.jsp?R=20170003687 2019-04-29T08:03:22+00:00Z

Climate Process Team on Internal-Wave Driven Ocean Mixing

Jennifer A. MacKinnon *

Scripps Institution of Oceanography, La Jolla USA

Matthew H. Alford

Scripps Institution of Oceanography, La Jolla USA

Joseph K. Ansong

Department of Earth and Environmental Sciences, University of Michigan, Ann Arbor USA

Brian K. Arbic

Department of Earth and Environmental Sciences, University of Michigan, Ann Arbor USA

Andrew Barna

Scripps Institution of Oceanography, La Jolla USA

Bruce P. Briegleb

National Center for Atmospheric Research, Boulder, CO USA

Frank O. Bryan

National Center for Atmospheric Research, Boulder, CO USA

Maarten C. Buijsman

Division of Marine Science, University of Southern Mississippi, Stennis Space Center, USA

Eric P. Chassignet

Center for Ocean-Atmospheric Prediction Studies, Florida State University, Tallahassee, USA

Gokhan Danabasoglu

National Center for Atmospheric Research, Boulder, CO USA

Steve Diggs

Scripps Institution of Oceanography, La Jolla USA

Stephen M. Griffies

NOAA Geophysical Fluid Dynamics Laboratory, Princeton USA

Robert W. Hallberg

NOAA Geophysical Fluid Dynamics Laboratory, Princeton USA

Steven R. Jayne

Woods Hole Oceanographic Institution, Woods Hole, Massachusetts, USA

Markus Jochum

Niels Bohr Institute, Copenhagen, Denmark

Jody M. Klymak

University of Victoria, Canada

Eric Kunze

Northwest Research Associates, Seattle, WA

William G. Large

National Center for Atmospheric Research, Boulder, CO USA

Sonya Legg

Program in Atmospheric and Oceanic Sciences, Princeton University, Princeton, USA

Benjamin Mater

Program in Atmospheric and Oceanic Sciences, Princeton University, Princeton, USA

Angelique V. Melet

Program in Atmospheric and Oceanic Sciences, Princeton University, Princeton, USA

Mercator Ocean, Ramonville St Agne, France

Lynne M. Merchant

Scripps Institution of Oceanography, La Jolla USA

Ruth Musgrave

Massachusetts Institute of Technology, Cambridge, USA

Jonathan D. Nash

Oregon State University, Corvallis, OR, USA

Nancy J. Norton

National Center for Atmospheric Research, Boulder, CO USA

Andrew Pickering

Oregon State University, Corvallis, OR, USA

Robert Pinkel

Scripps Institution of Oceanography, La Jolla USA

Kurt Polzin

Woods Hole Oceanographic Institution, Woods Hole, Massachusetts, USA

Harper L. Simmons

University of Alaska Fairbanks, Fairbanks, Alaska USA

Louis C. St. Laurent

Woods Hole Oceanographic Institution, Woods Hole, Massachusetts, USA

Oliver M. Sun

Woods Hole Oceanographic Institution, Woods Hole, Massachusetts, USA

David S. Trossman

Goddard Earth Sciences Technology and Research, Greenbelt, Maryland, USA

Department of Earth and Planetary Sciences, Johns Hopkins University, Baltimore USA

Amy F. Waterhouse

Scripps Institution of Oceanography, La Jolla USA

Caitlin B. Whalen

Applied Physics Laboratory, University of Washington, Seattle, Washington, USA

Zhongxiang Zhao

Applied Physics Laboratory, University of Washington, Seattle, Washington, USA

*Corresponding author address: 9500 Gilman Drive, M/C 0213, La Jolla, CA 92093

E-mail: jmackinnon@ucsd.edu

ABSTRACT

Diapycnal mixing plays a primary role in the thermodynamic balance of the ocean and, consequently, in oceanic heat and carbon uptake and storage. Though observed mixing rates are on average consistent with values required by inverse models, recent attention has focused on the dramatic spatial variability, spanning several orders of magnitude, of mixing rates in both the upper and deep ocean. Away from ocean boundaries, the spatio-temporal patterns of mixing are largely driven by the geography of generation, propagation and dissipation of internal waves, which supply much of the power for turbulent mixing. Over the last five years and under the auspices of US CLIVAR, a NSF- and NOAA-supported Climate Process Team has been engaged in developing, implementing and testing dynamics-based parameterizations for internal-wave driven turbulent mixing in global ocean models. The work has primarily focused on turbulence 1) near sites of internal tide generation, 2) in the upper ocean related to wind-generated near inertial motions, 3) due to internal lee waves generated by low-frequency mesoscale flows over topography, and 4) at ocean margins. Here we review recent progress, describe the tools developed, and discuss future directions.

1. Introduction

a. Context

Ocean turbulence influences the transport of heat, freshwater, dissolved gases such as CO_2, pollutants and other tracers. It is central to understanding ocean energetics and reducing uncertainties in global circulation and simulations from climate models. The dissipation of turbulent energy in stratified water results in irreversible diapycnal (across density surfaces) mixing. Recent work has shown that the spatial and temporal inhomogeneity in diapycnal mixing may play a critical role in a variety of climate phenomena. Hence a quantitative understanding of the physics that drive the distribution of diapycnal mixing in the ocean interior is fundamental to understanding the ocean's role in climate.

Diapycnal mixing is very difficult to accurately parameterize in numerical ocean models for two reasons. The first one is due to the discrete representation of tracer advection in directions that are not perfectly aligned with isopycnals, which can result in numerically induced mixing from truncation errors that is larger than observed diapycnal mixing (Griffies et al. 2000; Ilıcak et al. 2012). The second reason is related to the intermittency of turbulence, which is generated by complex and chaotic motions that span a large space-time range. Furthermore, this mixing is driven by a wide range of processes with distinct governing physics that create a rich global geography (see MacKinnon et al. (2013a) for a review). The difficulty is also related to the relatively sparse direct sampling of ocean mixing, whereby sophisticated ship-based measurements are generally required to accurately characterize ocean mixing processes. Nonetheless, we have sufficient evidence from theory, process models, laboratory experiments, and field measurements to conclude that away from ocean boundaries (atmosphere, ice, or the solid ocean bottom), diapycnal mixing is largely related to the *breaking of internal gravity waves*, which have a complex dynamical under-

pinning and associated geography. Consequently, in 2010, a Climate Process Team (CPT), funded by the National Science Foundation and the National Atmospheric and Oceanic Administration, was convened to consolidate knowledge on internal-wave-driven turbulent mixing in the ocean, develop new and more accurate parameterizations suitable for global ocean models, and consider the consequences for global circulation and climate. Here we report on the major findings and products from this CPT.

Ocean internal gravity waves propagate through the stratified interior of the ocean. They are generated by a variety of mechanisms, with the most important being tidal flow over topography, wind variations at the sea-surface, and flow of ocean currents and eddies over topography leading to lee-waves (see schematic in Figure 1). As waves propagate horizontally and vertically away from their generation sites, they interact with each other, producing an internal gravity wave continuum consisting of energy in many frequencies and wavenumbers. The waves with high vertical wavenumbers (small vertical scales) are more likely to break, leading to turbulent mixing. The distribution of diapycnal mixing therefore depends on the entire chain of processes shown in Figure 1.

b. A brief history of vertical mixing parameterizations used by ocean models

Ocean models often approximate diapycnal mixing processes through vertical Fickian diffusion, which takes the mathematical form

$$\text{Fickian diffusion} = \frac{\partial}{\partial z}\left(\kappa \frac{\partial \psi}{\partial z}\right), \tag{1}$$

where ψ is the tracer concentration, z is the geopotential vertical coordinate, and κ is the diapycnal diffusivity (dimensions of $L^2\ T^{-1}$). Through the 1990s, global models routinely used space-time constant vertical diffusivities. A notable exception was Bryan and Lewis (1979), who prescribed

a horizontally uniform diffusivity that increased with depth, reflecting the observed larger vertical mixing in the deep ocean and reduced mixing in the pycnocline. By the mid-1990s, ocean climate models began to separate diapycnal mixing into surface boundary layer and interior processes. In and near the surface boundary layer, mixing is controlled by a balance between buoyancy input (e.g., heat and freshwater fluxes) and mechanical forcing (e.g., wind) that establish the surface boundary layer and fluxes through it. Climate models of this era used boundary layer schemes such as Gaspar et al. (1990) and Large et al. (1994). In the stably stratified ocean interior, both shear-driven mixing (Pacanowski and Philander 1981; Large et al. 1994) and double-diffusive processes (Large et al. 1994) were parameterized. Gravitational instabilities giving rise to vertical convection were accounted for through a large vertical diffusivity (Large et al. 1994; Klinger et al. 1996) or a convective adjustment scheme (Rahmstorf 1993).

In the deep ocean, a prognostic parameterization for internal tide-driven mixing was introduced by St. Laurent et al. (2002), who combined an estimate of internal tide generation over rough topography with an empirical vertical decay scale for the enhanced turbulence (see Section 3). State-of-the-art ocean climate simulations prior to the CPT, as represented by the Geophysical Fluid Dynamics Laboratory (GFDL) and National Center for Atmospheric Research (NCAR) CMIP5 simulations (Dunne et al. 2012; Danabasoglu et al. 2012), included a version of equation (3) (see Section 3), along with parameterizations of mixing in the surface (Large et al. 1994) and bottom boundary layers and/or overflows (Legg et al. 2006; Danabasoglu et al. 2010), and mixing from resolved shear (Large et al. 1994; Jackson et al. 2008). These parameterizations produced spatially and temporally varying diapycnal diffusivities, with bottom enhancement and stratification dependence. However, these simulations did not include an energetically consistent representation of internal tide breaking away from the generation site; explicit representation of mixing from internal waves generated by winds and sub-inertial flows; nor spatial and temporal variability in the

dissipation vertical profile. The work described here has revolved around developing and testing energetically consistent, spatially and temporally variable mixing parameterizations. The resulting parameterizations are based upon internal gravity wave dynamics and the patterns of wave generation, propagation, and dissipation.

c. Overall strategy and philosophy of the CPT approach

As with previous CPTs, we have found that parameterizations are most productively developed when there is a broad base of knowledge that is in a state of *readiness* to be consolidated, implemented and tested. Much of the basic research described here was published or nearing completion at the time this project started, allowing for a focused effort on parameterization development, model implementation and global model testing. A key CPT component was the inclusion of four dedicated post-doctoral scholars, who formed "the glue" to bridge the expertise of different principal investigators, promoting projects at the intersection of theory and models, observations and simulations, while gaining valuable broad training and networking.

One of the important tenets of the CPT is the consistent use of energy, power and the turbulent kinetic energy dissipation rate ε (dimensions of $L^2\ T^{-3}$), rather than diapycnal diffusivity, as the currency of turbulent mixing. ε describes the rate at which turbulence dissipates mechanical energy at the smallest scales. It is typically related to a diapycnal diffusivity through a dimensionless mixing efficiency (Γ), following Osborn (1980)

$$\kappa = \frac{\Gamma \varepsilon}{N^2}, \tag{2}$$

where N^2 is the squared buoyancy frequency. Equation (2) shows that keeping the diffusivity fixed in a world with changing stratification implies changes in energy dissipation in ways that are not always consistent with the physical processes supplying energy for dissipation. We can overcome

this problem by formulating parameterizations directly in terms of ε. This approach also has the advantage of providing a transparent connection to dynamical processes driving mixing, since the downscale energy cascade can be directly linked to constraints of total power available for turbulence and other facets of ocean energetics (e.g., St. Laurent and Simmons 2006; Ferrari and Wunsch 2009). The topic of an appropriate value for mixing efficiency has had a resurgence of interest in recent years. Some theoretical and numerical studies suggest that a mixing efficiency that is systematically lower in areas of low ocean stratification might bias the type of global mixing estimates presented here and require modifications to model parameterizations (Mashayek et al. 2013; Venayagamoorthy and Koseff 2016; Salehipour et al. 2016). A careful evaluation of mixing efficiency was not part of the CPT work, and a thorough discussion is beyond the scope of this paper. Interested readers are instead referred to recent reviews such as Peltier and Caulfield (2003) and Gregg et al. (2017).

2. Global patterns and constraints

Many of the early parameterizations described in Section 1b were motivated by individual process experiments or observational studies. At the same time, the novel observations, theories, and model results that fundamentally drive the field forward frequently arise unexpectedly, from programs funded by many agencies. For example, the long-range propagation of coherent internal tides was discovered in both the ATOC (Acoustic Thermometry of Ocean Climate; Dushaw et al. (1995)) and satellite altimeter (Ray and Mitchum 1996) datasets fortuitously–neither mission was set up with a focus on internal tides.

Another factor contributing to the readiness of this CPT was the increased use of new techniques to infer mixing rates indirectly from a wide variety of data sources, allowing the rich patterns like those in Figure 2 to emerge. There are now enough direct microstructure and indirect estimates of

turbulent dissipation rates and diapycnal diffusivities to examine depth and geographical patterns, temporal variability and global budgets (Waterhouse et al. 2014). These patterns in turn have inspired new insights on the underlying dynamics driving and energetically supplying small-scale turbulence, and provided valuable constraints on modeled turbulent mixing rates. Compilation of both direct microstructure measurements and indirect estimates of turbulence is discussed in Section 7. Here we briefly describe recent results related to global patterns and statistics.

The average strength of turbulent diapycnal mixing appears to be roughly consistent, within error bars, with that 'required' to raise the deep waters of the global meridional overturning circulation (MOC). Using the most comprehensive-to-date collection of full-depth microstructure data, Waterhouse et al. (2014) report a globally-averaged diapycnal diffusivity below 1000 m depth of $\mathscr{O}(10^{-4}\ \mathrm{m}^2\ \mathrm{s}^{-1})$ and above 1000 m depth of $\mathscr{O}(10^{-5}\ \mathrm{m}^2\ \mathrm{s}^{-1})$. These values are consistent with the global inverse estimate of Lumpkin and Speer (2007). Using an indirect finescale approach (Section 7c), but with a much larger dataset, Kunze (2017) finds a global depth-averaged value of $0.3 - 0.4 \times 10^{-4}\ \mathrm{m}^2\mathrm{s}^{-1}$. It is unclear whether any remaining differences between these estimates are due to sampling biases of the more limited microstructure data, to method biases of the finescale technique, or to assumptions of a fixed mixing efficiency.

The associated globally-averaged turbulent dissipation rates inferred from these observations cluster around 2 ± 0.6 TW (Waterhouse et al. 2014; Kunze 2017). Given an assumed mixing efficiency, these rates are roughly consistent with estimates of power going through the three primary mechanisms of internal wave generation: barotropic tidal flow over topography leading to internal tides ($\sim$ 1 TW, see Sections 3 and 4); low-frequency flows over topography producing internal lee waves (0.2–0.7 TW, see Section 5); and variable wind forcing producing near-inertial internal waves ($\sim$ 0.3–1 TW, see Section 6).

Much more striking than average values is the enormous range and richness of the patterns visible in Figure 2. Both the turbulent dissipation rate and diapycnal diffusivity vary by several orders of magnitude across ocean basins. Understanding how such patterns convolve with pathways of water mass movement, air-sea heat gain/loss, greenhouse gas input, and nutrient availability is the next frontier in interpreting diapycnal mixing in the ocean.

Many of these patterns (in space and time) can be interpreted in terms of the geography of internal wave generation, propagation, and dissipation (Figure 1). Patterns immediately visible in Figure 2 include elevated values associated with more complex topography such as that associated with the western Indian, western and central Pacific and slow mid-ocean spreading ridges (Wijesekera et al. 1993; Polzin et al. 1997; Kunze et al. 2006; Decloedt and Luther 2010; Wu et al. 2011; Whalen et al. 2012; Waterhouse et al. 2014). Over rough or steep topography, turbulence is frequently bottom-enhanced (Polzin et al. 1997; Waterhouse et al. 2014), but sometimes extends all the way up through the pycnocline (Kunze 2017). The temporal variability of diapycnal mixing shows seasonal (Whalen et al. 2012) and tidal cycles related to the two major internal wave energy sources, the winds and tides, as well as isolated events.

What follows in the sections below concerns first the main science efforts to consolidate our understanding of turbulence from (i) mixing elevated over rough topography related to internal wave generation by tides, (ii) low-frequency flows that generate internal lee waves, and (iii) near-inertial internal wave generation by winds. In each section we describe the consequences of parameterizing these processes in ocean climate models. For tides we subdivide our efforts into turbulence in the 'nearfield' of internal tide generation sites (loosely within one mode-one bounce) and the 'farfield' (waves that have propagated considerably further before breaking). Following that we describe tools developed through the CPT now made available to the wider community; namely (1) a uniquely comprehensive database of microstructure data, (2) techniques for analyzing ob-

servational data, and (3) new parameterizations of turbulence available for a variety of model implementations. We also briefly discuss the state of the art for high-resolution ocean models, which are beginning to partially resolve the internal gravity wave continuum on a global scale. We conclude this paper with thoughts for the future.

3. Nearfield tidal mixing

a. Physical motivation

Tidal frequency internal waves, generated by barotropic tidal flow over topographic obstacles in a stably stratified fluid, lead to local mixing near the generation site, both due to direct wave breaking (close to topography) and enhanced rates of interaction with other internal waves (well above topography). The formulation of St. Laurent et al. (2002) represented the enhanced turbulent dissipation rate as the product of the rate of conversion of barotropic tidal energy into internal waves, C; the fraction of that energy which is 'locally' dissipated, q (note that consequently $1-q$ propagates away as low-mode internal tides); and a vertical distribution function of that local dissipation, $F(z)$. Through the Osborn relation in equation (2) (Osborn 1980), the enhanced turbulence is then related to a diffusivity as

$$\kappa = \kappa_b + \frac{q\Gamma C(x,y)F(z)}{\rho N^2}, \tag{3}$$

where κ_b is a place-holder background diffusivity. The conversion rate, C, is dependent on topographic roughness, tidal velocity, and bottom stratification (Bell 1975; Jayne and St. Laurent 2001; Garrett and Kunze 2007) (Figure 3c). St. Laurent et al. (2002) proposed a value of $q = 1/3$, and a function $F(z)$ that decayed exponentially with height above topography, with a 500 m e-folding scale. They based these choices on analysis from several deep-ocean microstructure datasets. These values were used in climate model implementations, such as Simmons et al. (2004b), Jayne

(2009), Dunne et al. (2012), and Danabasoglu et al. (2012). The background diffusivity, κ_b, accounts for the mixing associated with energy that radiates from internal-tide generation sites, as well as other internal wave processes. Treatments of κ_b have varied, including: (i) a constant value of 1×10^{-5} m^2 s^{-1} (Simmons et al. 2004b; Jayne 2009), (ii) a latitudinal function capturing the equatorward decrease in wave-wave interactions (Henyey et al. 1986; Harrison and Hallberg 2008; Jochum 2009; Danabasoglu et al. 2012), and (iii) a stratification-dependent function after Gargett (1984) (used in Dunne et al. (2012)). Due to the sensitivity of the simulations to the different parameterizations, a major goal of the CPT has been to better understand and represent the physical processes that determine spatial and temporal variations in the parameters in equation (3).

A few estimates of q have been obtained, involving synthesis of observations and models. The radiated portion $1-q$ may be computed as the energy radiated out of a control volume $\int \boldsymbol{J} \cdot \hat{\boldsymbol{n}}\, dA$, where $\boldsymbol{J}$ is the internal wave energy flux, divided by an estimate of the conversion rate C. Alternately, a direct estimate is from the integrated dissipation rate over that same volume, $\int \rho \Gamma \varepsilon dV / C$. The observational sampling requirements for both estimates, particularly the second, are considerable. At the Hawaiian ridge, Klymak et al. (2006) obtained $q = 0.15$ using the second method, as compared to an estimate of $q < 0.5$ obtained with the first (Rudnick et al. 2003).

Existing theoretical predictions for C, summarized in Garrett and Kunze (2007) and Green and Nycander (2013), show dependence on topographic steepness relative to the internal tide characteristic steepness $\gamma = (dh/dx)/s$ (where $s = \sqrt{(f^2-\omega^2)/(N^2-\omega^2)}$, dh/dx is the topographic gradient, ω is the wave frequency and f the Coriolis parameter), as well as the ratio of tidal excursion distance to topographic width. At supercritical rough topography ($\gamma > 1$) the conversion rate saturates (Balmforth and Peacock 2009; Zhang and Swinney 2014) compared to linear theory applicable at subcritical topography ($\gamma < 1$) (Bell 1975). Estimates of C need to include the contribution of abyssal hill topography, on scales $\mathscr{O}(< 10$ km) not resolved by current topography

products. Small-scale topography may increase C by 10% globally and 100% regionally (Melet et al. 2013b) (see Figure 3c).

A global constraint on the nearfield internal tide dissipation can be obtained from comparisons of satellite observations of internal tides with global simulations at $\mathcal{O}(10\text{ km})$ resolution that include realistic surface tidal forcing (Simmons et al. 2004a; Arbic et al. 2004, 2010; Niwa and Hibiya 2011; Müller et al. 2012; Shriver et al. 2012; Niwa and Hibiya 2014; Shriver et al. 2014; Waterhouse et al. 2014; Ansong et al. 2015; Buijsman et al. 2016; Rocha et al. 2016). All of these model runs explicitly simulate generation of low-mode tides, with horizontal scales $> \mathcal{O}(50)$ km. Some studies conducted since 2010 have also included concurrent atmospheric forcing, allowing for a more realistic, geographically varying background stratification field. In some of the models above, conversion to unresolved high modes, assumed to dissipate locally, is performed by a linear wave drag based on linear theory (Bell 1975). Buijsman et al. (2016) find that modeled and observed internal tides show most agreement when about 60% of the energy converted to both low and high modes is dissipated close to the generation sites.

The vertical structure of associated turbulence appears to vary between deep rough topography, and tall steep topography, reflecting differences in the underlying physics driving turbulence. At tall steep ridges much of the baroclinic energy is contained in larger length scales that propagate away horizontally without breaking (St. Laurent and Nash 2004). Local mixing occurs through tidally generated transient arrested lee waves (Legg and Klymak 2008; Klymak et al. 2010; Alford et al. 2014) (Figure 3b), which might imply a q scaling with the barotropic flow speed U, and an exponentially decaying vertical dissipation profile with lengthscale U/N. At the Kaena ridge, Hawaii, this theory suggests $q \sim 7\%$, less than the $q \sim 15\%$ values estimated from observations (Klymak et al. 2006). Interference with remotely generated internal tides modifies the local dissipation (Buijsman et al. 2012, 2014; Klymak et al. 2013); resonance between internal tides

generated at adjacent ridges (e.g. Luzon Straits) can increase local dissipation up to 40% (Alford et al. 2015). The percentage of local dissipation may be systematically higher in marginal seas or areas where lower modes are not free to escape (St. Laurent 2008; Nagai and Hibiya 2015). Similarly, nearfield tidal dissipation can be increased by topographically trapped internal waves generated by subinertial tidal constituents (Tanaka et al. 2013); i.e., the diurnal constituents at latitudes $> 30°$, and the semidiurnal constituents at latitudes $> 74.5°$. The energy density in such trapped motions increases with latitude, and is all dissipated locally (Musgrave et al. 2016).

At deep rough topography a variety of processes facilitate local wave breaking (Figure 3a). Wave-wave interactions can transfer energy to smaller scale waves that are more likely to break (McComas 1977; Müller et al. 1986; Henyey et al. 1986). This process is modeled in Polzin (2004b) with a one-dimensional radiation balance equation, resulting in an algebraically decaying dissipation profile with a spatially varying decay scale that matches Brazil Basin observations (Polzin et al. 1997) (Figure 3d). For small scale waves generated over subcritical abyssal hill topography, overturning of the upward propagating waves (Muller and Bühler 2009), predicts a bottom intensified dissipation, with a steeper than exponential decay with height and a local dissipation fraction as large as 60%. At and just below a critical latitude where the Coriolis frequency is half the tidal frequency, particularly efficient wave-wave interactions of a parametric subharmonic instability type lead to a dissipation profile with high values extending several hundred meters above the bottom, before decaying rapidly to background levels, and $q > 0.4$ (MacKinnon and Winters 2003; Ivey et al. 2008; Nikurashin and Legg 2011). Internal tide energy can also be transferred to smaller scales in the pycnocline, and by scattering from rough topography following reflection from the upper surface (Buhler and Holmes-Cerfon 2011). The value of $q = 0.3$ used in existing parameterizations is therefore likely to be an under-estimate in many places, while an over-estimate in some.

b. New parameterizations

A major effort in the CPT and elsewhere has been to build upon the work of Jayne and St. Laurent (2001) and St. Laurent et al. (2002) by deriving more dynamically variable and accurate representations of both the decay profile, $F(z)$, and the fraction of locally dissipated wave energy, q. For deep, rough topography, Polzin (2009) formulates a parameterization of internal tide dissipation based on 1-D radiation balance equations with nonlinear closure. His formulation yields a dissipation that scales like $\varepsilon = \varepsilon_0/(1+z/z_p)^2$, where z is the height above bottom (Figure 3d). In Melet et al. (2013a) the scale height z_p is written in the form

$$z_p = \mu \left(\frac{U\,(N_b^{\mathrm{ref}})^2}{h^2 k^2 N_b^3} \right) \tag{4}$$

where μ is a non-dimensional constant, N_b^{ref} is a reference bottom buoyancy frequency, and U, h, k, and N_b are respectively the barotropic velocity, topographic roughness, topographic wavenumber, and bottom buoyancy frequency for the particular location. WKB scaling contributes to the role of stratification in (4). Another global map of q and vertical profile of dissipation for small-scale rough topography has been generated by Lefauve et al. (2015) using the overturn mechanism of Muller and Bühler (2009).

For turbulence at tall, steep slopes, a new parameterization of the near-field mixing due to transient arrested lee-waves (Klymak et al. 2010) uses linear theory for knife-edge ridge topography to estimate baroclinic energy conversion into each mode (Llewellyn Smith and Young 2003). Those modes with phase speeds less than the barotropic velocity at the top of the ridge are assumed to be arrested, leading to local dissipation. Combining the total energy loss with a vertical length scale of U/N produces a dissipation rate which decays exponentially away from the ridge top.

c. Consequences for large-scale circulation

Melet et al. (2013a) compare two simulations with the same formulation for internal-tide energy input but using different vertical profiles of dissipation (the St. Laurent et al. (2002) and Polzin (2009) formulations, also included in the Community Earth System Model, CESM). They used the GFDL CM2G coupled climate model with an isopycnal vertical coordinate in the ocean (Dunne et al. 2012). With the Polzin formulation, diffusivities are higher around 1000–1500 m, and lower in the deep ocean, resulting in modifications to the ocean stratification and changes of $\mathcal{O}(10\%)$ in the meridional overturning circulation (Figure 3e).

Additional enhancements in the CESM ocean component, meant to improve the representation of tidally-driven mixing, include: separate treatment of diurnal and semi-diurnal tidal constituents and implementation of a subgrid-scale bathymetry parameterization that better resolves the vertical distribution of the barotropic energy flux, following Schmittner and Egbert (2014); alternative tidal dissipation energy data sets from Egbert and Ray (2003) and Green and Nycander (2013); and introduction of the 18.6-year lunar nodal cycle on the tidal energy fields. The global climate impacts of these new enhancements are found to be rather small. However, there are local improvements such as a reduction in the warm bias in the upper ocean in the Kuril Strait region.

d. Future work

Ongoing work is synthesizing existing ideas for the dependence of q on topographic and flow parameters into a single global model for a spatially and temporally varying q, and incorporating these ideas into simulations. Comparison with additional observations of the strength and vertical decay scale of turbulence over rough topography is also desirable. For example, Kunze (2017) find that inferred dissipation rates over some topographic features extend upwards well into the ther-

mocline without appreciable decay. Parameterization of mixing by trapped tidally forced waves (perhaps especially important in the Arctic and Antarctic) also deserves dedicated attention.

4. Farfield internal tides

About 20–80% of the internal tide energy is not dissipated near topographic sources (Section 3), and instead radiates away as low-mode internal waves. Satellite altimetry shows that these low-mode internal tides may propagate for thousands of kilometers from sources such as the Hawaiian Ridge (Figure 4*a*; Zhao et al. (2016)). This section examines where and how these low-modes dissipate, and parameterizations of this dissipation. Several mechanisms have been hypothesized as potential dissipators of farfield internal tides, including: interactions with rough topography (Johnston and Merrifield 2003; Mathur et al. 2014), interactions with mean flows and eddies (St. Laurent and Garrett 2002; Rainville and Pinkel 2006; Dunphy and Lamb 2014; Kerry et al. 2014), cascade to smaller scales via wave-wave interactions (McComas 1977; Müller et al. 1986; Henyey et al. 1986; Lvov et al. 2004; Polzin 2004a), including the particular subset of wave interactions known as parametric subharmonic instability (PSI) (Staquet and Sommeria 2002; MacKinnon and Winters 2005; Alford et al. 2007; Alford 2008; Hazewinkel and Winters 2011; MacKinnon et al. 2013b,c; Simmons 2008; Sun and Pinkel 2012, 2013), or evolution on continental slopes and shelves (Nash et al. 2004, 2007; Martini et al. 2011; Kelly et al. 2013; Waterhouse et al. 2014). Here we summarize current understanding from theoretical and process studies and observational campaigns, recent parameterization developments, and consequences of farfield dissipation for global ocean models.

a. Observations

The reflection, scattering, and dissipation of long-range low-mode internal tides have been observed at a few large topographic features. Satellite altimetry indicates scattering of mode-1 tides to higher modes along the Line Islands Ridge, 1000 km south of Hawaii (Johnston and Merrifield 2003). Moored observations show significant reflection for mode-1 diurnal internal tides (but weak reflection for semidiurnal) at the South China Sea continental shelf (Klymak et al. 2011). Scattering of internal tides from low to high modes, and associated mixing, has been observed on the Virginia and Oregon continental slops (Nash et al. 2004; Kelly et al. 2012; Martini et al. 2013). In contrast, at the steeper Tasmanian continental slope mode-1 internal tides appear to reflect without significant energy loss (Johnston et al. 2015).

b. Theory and numerical simulations

The interaction between low-mode internal waves and large-amplitude topography, such as continental slopes or tall isolated ridges, is strongly dependent on the steepness of the topography (Cacchione and Wunsch 1974; Johnston and Merrifield 2003; Legg and Adcroft 2003; Venayagamoorthy and Fringer 2006; Helfrich and Grimshaw 2008; Hall et al. 2013; Legg 2014; Mathur et al. 2014). Shoaling subcritical topography can increase wave amplitude, increasing the Froude number (defined in Section 5) and causing wave breaking. Supercritical topography reflects low-mode waves back towards deeper water, with only small energy loss to dissipation (Klymak et al. 2013). Near-critical topography scatters incident low-mode energy to much smaller wavelengths, leading to wave breaking and turbulence (Wunsch 1969; Ivey and Nokes 1989; Slinn and Riley 1996; Ivey et al. 2000) concentrated near the sloping topography. Kelly et al. (2013) estimated the fraction of incoming mode-1 energy flux transmitted, reflected and scattered into higher modes for 2-dimensional sections across the continental slope for the entire global coastline. Three-

dimensional topographic variations such as canyons, cross-slope ridges and troughs, and bumps may enhance the local dissipation of the low-mode tide.

c. Parameterizing farfield tides: a wave drag approach

In global simulations of the HYbrid Coordinate Ocean Model (HYCOM) with realistic atmospheric and tidal forcing (Arbic et al. 2010), the resolved internal waves lose energy to a wave drag applied to flow in the bottom 500 m (see Section 3). This drag can be regarded as a parameterization of low- to high-mode scattering, and these high modes are assumed to dissipate at the generation site, within 500 m above the bottom topography. Comparison of the simulated M_2 internal-tide SSH amplitudes in $1/12.5°$ HYCOM with satellite altimetry (Shriver et al. 2012; Ansong et al. 2015; Buijsman et al. 2016), shows that the open ocean wave drag is necessary to achieve agreement between modeled and observed barotropic and baroclinic tides, confirming the need for deep ocean dissipation of the low mode internal tides. Figures 4*b* and 4*c*, taken from Ansong et al. (2017), display the internal tide conversion rates and fluxes in HYCOM, and the comparison of HYCOM fluxes to fluxes in high-vertical-resolution moorings in the North Pacific (Zhao et al. 2010). Consistent with earlier studies, such as Simmons et al. (2004a), the conversion map shows that internal tides are generated in areas of rough topography such as the Hawaiian Ridge. The HYCOM-mooring comparison map in Figure 4*c* indicates that the HYCOM simulations are able to predict tidal fluxes with some reasonable degree of accuracy. Buijsman et al. (2016) found that about 12 % of these low modes reach the continental slopes, compared to 31 % found by Waterhouse et al. (2014). The HYCOM results cited above suggest the necessity of parameterized energy loss; but the current wave drag formulation used in HYCOM is based only upon topographic scattering, motivating additional studies to understand a greater number of relevant physical mechanisms implicated in the damping of farfield internal tides.

d. Parameterizing farfield internal tides: a ray-tracing approach

To represent the geography of farfield internal tide dissipation in a physically-based manner, the propagation, reflection and dissipation of low-mode energy must be parameterized in a GCM. A new numerical framework employs a vertically-integrated radiation balance equation to predict the horizontal propagation of low-mode energy, simplifying earlier surface and internal wave modeling (e.g., WAMDI-Group 1988; Müller and Natarov 2003). In this approach, only the lowest modes are considered. Energy in each mode of each relevant tidal frequency is considered independently (or adiabatically), assuming minimal mode-mode energy transfer. Waves propagate horizontally with refraction due to variations in Coriolis, depth and stratification, invoking classic ray-tracing equations for long internal gravity waves (Lighthill 1976). Effects of background flow (Rainville and Pinkel 2006) are currently neglected, but will be included in future versions. The $1-q$ fraction of the outgoing internal tide energy that does not dissipate locally (see Section 3) forms the source term in the radiation balance equation, and various parameterizations for dissipation can be "plugge into" the framework as sink terms. Dissipation mechanisms currently considered include scattering at small-scale roughness (Jayne and St. Laurent 2001), quadratic bottom drag (similar to some of the simulations in Ansong et al. (2015)), and Froude number-based breaking (Legg 2014). A scheme for partial reflection at continental slopes uses the reflection coefficients of Kelly et al. (2013). This framework, currently implemented in GFDL's MOM6 ocean model, can be adapted or extended to incorporate new parameterizations of sink and source phenomena. Eden and Olbers (2014) have developed a similar approach for propagating low-mode energy, with scattering to a high-mode continuum due to wave-wave interaction and topographic roughness (not including reflection at continental slopes).

e. Consequences of farfield dissipation in GCMs

To examine the sensitivity of large-scale ocean circulation to the location of farfield internal tide dissipation, a series of simulations were performed with the GFDL ESM2G coupled climate model (Dunne et al. 2012). These simulations (Melet et al. 2016) all have the same total energy input into the internal tide field, and the same magnitude and location of nearfield dissipation, with $q = 0.2$ and the bottom-intensified vertical profile described in St. Laurent and Garrett (2002). The remaining 80 % of energy dissipation is distributed at one of three horizontal locations — deep basins, continental slope, coastal shelves — with one of three vertical dissipation profiles – dissipation which decays exponentially with height above bottom, scales like the buoyancy frequency N, or like N^2 (see Melet et al. (2016) for more detail). The resulting ocean circulation shows a significant dependence on the vertical profile of dissipation (Figures 4e and 4f). In particular, more dissipation in the upper ocean leads to stronger subtropical overturning cells, a broader thermocline, and higher thermosteric sea-level; more dissipation in the deep ocean leads to stronger deep meridional overturning circulation (more evidence of these impacts is shown in Melet et al. (2016)). In addition, the geographic location of the farfield dissipation influences the large-scale circulation notably when it impacts dense water formation regions: more dissipation on the slopes and shelves near the descending overflows tends to weaken the meridional overturning cell for which the lower branch is supplied by the overflows.

f. Future work

Future work on the ray-tracing approach should include refinement of the directional spectrum of radiated low-mode waves, including refraction by background flow, and evaluation of its impact in GCMs. Further work is also needed to understand and incorporate some of the detailed mechanisms of internal tide dissipation. One of these mechanisms is PSI, which may be especially

important near and equatorward of the diurnal turning latitudes $\sim$29°N/S. Note that the tide energy pathways via the tide constituents S_2, O_1, and K_1, which collectively account for an amount of energy comparable to that of M_2 (even greater, in some regions), need to be better understood. In particular, internal tides of various frequencies may have different responses to the same bottom topography and time-varying background flow. Progress here will involve a combination of relevant theory and observations with both idealized simulations and realistic tidally forced global simulations. Another dissipation pathway worthy of close attention is wave breaking and turbulence on continental slopes and shelves, where the vertical structure may be heavily influenced by details of wave dynamics in the presence of small-scale coastal topography, in ways that are not yet fully understood (e.g., Nash et al. 2007; Kunze et al. 2012; Wain et al. 2013; Pinkel et al. 2015; Waterhouse et al. 2017).

5. Internal lee waves

a. Theory and observations

As with tides, mean flows over rough topography can generate internal waves that can remove energy and momentum from the large-scale circulation and, when they break, produce turbulent mixing (Figure 5a). Quasi-steady flow over small amplitude bathymetry ($\gamma \lesssim 1/2$, Nikurashin et al. (2014)) gives rise to vertically propagating internal lee waves of frequency Uk, where k is the topographic horizontal wavenumber and U is the mean flow speed. For large amplitude topography ($\gamma \gtrsim 1/2$), the Froude number of the flow $F = U/NH$ is $\mathscr{O}(1)$, such that topographic flow blocking and splitting becomes prominent: the flow transits the bump generating a non-propagating disturbance that converts parts of the flow kinetic energy to dissipation. Most of the real ocean lies between these two end cases (Bretherton 1969; Bell 1975; Pierrehumbert and

Bacmeister 1987; St. Laurent and Garrett 2002). The drag due to the combination of internal lee wave generation and topographic flow blocking and splitting is commonly denoted as wave drag in the atmospheric literature. Parameterizations of wave drag have been used for a long time in the atmospheric community (e.g. Palmer et al. 1986) but are less common in the ocean community.

Available global estimates for the energy conversion rate from geostrophic flows into internal lee waves range from 0.2 to 0.75 TW and highlight a prominent role of the Southern Ocean (Bell 1975; Nikurashin and Ferrari 2011; Scott et al. 2011; Wright et al. 2014). Several lines of evidence have suggested the existence of propagating lee waves (e.g., Naveira Garabato et al. 2004; St. Laurent et al. 2012; Waterman et al. 2013; Sheen et al. 2013, 2014; Clement et al. 2016) (Figure 5a). Yet, lee waves have not been definitively identified in ocean observations until recently, with Cusack et al. (2017) reporting unambiguous evidence of a lee wave in the Drake Passage (the search is complicated in part by the difficulty of observing motions with zero Eulerian frequency). Sparse observations also make it difficult to determine the fate of propagating lee waves. Non-propagating lee waves have been observed in a variety of fracture zones and deep passages (Ferron et al. 1998; Thurnherr et al. 2005; MacKinnon 2013; Alford et al. 2013), but their integrated importance to abyssal mixing is unknown.

b. Parameterizations and consequences of lee wave driven mixing on the ocean state

The sensitivity of large-scale ocean circulation to lee wave driven mixing has been investigated in simulations with the GFDL ESM2G coupled climate model (Melet et al. 2014) using the estimated global map of energy conversion into lee waves of Nikurashin and Ferrari (2011) (Figure 5b). The St. Laurent et al. (2002) exponential vertical structure was used as an initial placeholder for the structure of dissipation associated with breaking lee waves. Although most estimates put the global energy input into lee waves smaller than that into internal tides, Melet et al. (2014)

showed that lee wave-driven mixing significantly impacts the ocean state, yielding a reduction of the ocean stratification associated with a warming of the abyssal ocean. The lower cell of the MOC is also slightly lightened and increased in strength (Figure 5c). The different spatial distribution of the internal tide and lee wave energy input is largely responsible for the sensitivity described in Melet et al. (2014), highlighting the previously reported importance of the patchiness of internal wave driven mixing in the ocean (e.g. Simmons et al. 2004a; Jayne 2009; Friedrich et al. 2011). Using a hydrographic climatology and a similar parameterization for lee wave driven mixing, Nikurashin and Ferrari (2013) and De Lavergne et al. (2016) also show substantial water mass transformation in the Southern Ocean due to internal lee wave driven mixing.

Trossman et al. (2013, 2016) implemented an inline wave drag parameterization (for both propagating and non-propagating lee waves) from the atmospheric community (Garner 2005) into a high-resolution ocean general circulation model (Figure 5d). The inline implementation allows for feedbacks between wave drag and the low-frequency flows that produce the lee waves. They found that the wave drag dissipated a substantial fraction of the wind energy input, significantly reduced both kinetic energy and stratification near the bottom, and reduced the model sea surface height variance and geostrophic surface kinetic energy by measurable amounts of $\sim$20%, while the performance of the model relative to in-situ and altimetric measurements of eddy kinetic energy was not negatively impacted. Trossman et al. (2015) showed that dissipations predicted by the Garner (2005) scheme are not inconsistent with microstructure observations within the bottom 500 meters in two Southern Ocean regions.

c. Future work

More observations are needed, especially in the Southern Ocean, to provide definitive evidence of the extent of propagating lee waves in the ocean, and further to explore (1) the fraction of

local dissipation and the vertical profile of dissipation of the propagating drag, (2) the relative importance of the propagating and non-propagating lee-wave drag, and (3) the observed mismatch between estimates of lee wave energy generation and near-bottom dissipation of lee waves.

Enhancing our knowledge of the near-bottom stratification and velocity fields and using a more accurate representation of topographic blocking are crucial for reducing our uncertainty about the global conversion rate into lee waves. Indeed, Wright et al. (2014) found that the use of different stratification products yields a difference of up to 0.25 TW in the global conversion rate into lee waves. Conversion rates are even more sensitive to the near-bottom velocity field (Trossman et al. 2013; Melet et al. 2015), which can vary drastically with model resolution (Thoppil et al. 2011) and should take into account mesoscale eddy velocities. Topographic blocking accounts for most of the predicted dissipation by the Garner (2005) scheme in the bottom 1000 meters of two Southern Ocean domains (Trossman et al. 2015). Recent laboratory experiments by Dossmann et al. (2016) have shown that, for most forcing parameters they considered, nonlinear mixing mechanisms close to abyssal topography, such as topographic blocking, dominate the remote mixing mechanism by lee waves. Yet, theoretical conversion rates are highly sensitive to the choice of uncertain parameters related to the representation of topographic blocking and splitting (Nikurashin et al. 2014).

As parameterized lee wave drag makes a significant impact on the ocean state (Trossman et al. 2013, 2016), it should be included inline within climate models in a dynamically accurate manner to ensure credible ocean representation in a changing climate. Using linear theory and modeled resolved and parameterized bottom velocities and stratification, Melet et al. (2015) showed that the energy flux into lee waves exhibits a clear annual cycle in the Southern Ocean and that the global energy flux is projected to decrease by $\sim$20% from pre-industrial to future climate conditions under the RCP8.5 scenario. This time-variability is primarily due to changes in bottom velocities

(Melet et al. 2015). Ultimately, models should aspire to a full coupling between wind power, eddies and geostrophic circulations, stratification, and lee-wave drag and induced mixing. Such a coupling requires a state dependent, time evolving parametrization for the effects of lee waves.

6. Wind-driven near-inertial motions

a. Theory and observations

Much of what is known about wind-generated near-inertial waves (NIWs) builds on the observations and model studies of the Ocean Storms Experiment (D'Asaro et al. 1995; Dohan and Davis 2011); for a summary of the outcomes, other generation mechanisms and additional studies (see a review by Alford et al. (2016)). Inertial oscillations of the boundary layer are a free mode of the ocean and are its first response to changes in the wind stress (e.g. D'Asaro 1985). Part of the inertial oscillation energy is dissipated in the boundary layer through shear instability, thus converting kinetic energy to heat and potential energy (Large and Crawford 1995), with the remainder radiated away downward (Figure 6a) and equatorward (Figure 6b) in the form of propagating near-inertial internal waves (Alford 2003a; Plueddemann and Farrar 2006; Alford et al. 2012; Simmons and Alford 2012). The partition between high and low modes and the energy lost to dissipation at the mixed-layer base is unknown. In Ocean Storms, approximately one third of the energy input by the wind was carried away equatorward in modes one and two. Another study (Alford et al. 2012) found a similar fraction was carried downward in higher modes, while a modeling study by Furuichi et al. (2008) found that only 10% reached past 150 m. Inferred global upper ocean dissipation rates show a clear seasonal cycle (Whalen et al. 2012), particularly in storm track latitudes (Whalen et al. 2015). Near-inertial KE at all depths also shows a clear seasonal cycle, indicating

that some of the energy makes it deep into the ocean (Alford and Whitmont 2007; Silverthorne and Toole 2009).

b. Parameterizations and consequences

The CPT tackled the upper ocean portion of the NIW related mixing with a three step process, described in Jochum et al. (2013), suitable for general use in coupled atmosphere-ocean models. Firstly, atmosphere and ocean models are coupled more frequently (e.g., two hours instead of daily), to allow resonant generation of near-inertial motions in the oceanic surface boundary layer. Even with high-frequency coupling, the near-inertial speeds can be too weak by 50% if the frontal structure of storms is not properly resolved by the atmospheric component of climate models. In such cases, the missing amplitude of the NIWs must be computed during the integration and added to the shear calculation of the boundary layer parameterization. The online computation of the near-inertial part of the velocity is not trivial, because during the integration the ocean model only has information about adjacent time steps. Fortunately, however, outside the deep tropics, velocity fluctuations from one model time step (e.g., one hour) to the next are mostly due to NIWs, which allows the accurate determination of near-inertial velocity during the integration (see Jochum et al. (2013) for details and method verification). Lastly, the air-sea flux of inertial wave energy into the boundary layer is determined, and 30% of it (Rimac et al. 2016) is used to increase the background diffusivity below the boundary layer. The energy in the last step is distributed with an exponential decay scale of 2000 m (Alford and Whitmont 2007). The resultant turbulent mixing from near-inertial motions changes the heat distribution in the upper ocean significantly enough to modify tropical SST patterns, and leads to a 20% reduction in tropical precipitation biases (Jochum et al. (2013); for the sensitivity of precipitation to the strength of near-inertial waves see Figures 6c and 6d).

c. Ongoing and future work

Much hinges on the appropriate representation of NIWs. The largest uncertainties are associated with the poorly known high frequency and wavenumber part of the wind spectrum, and the partitioning between locally dissipated energy and the amount radiated away. Thus, the energy available for NIW induced mixing in the surface boundary layer ranges from 0.3-1.0 TW (Alford 2001, 2003b; Simmons and Alford 2012; Rimac et al. 2013). The Jochum et al. (2013) study was based on 0.34 TW; allowing for 0.68 TW in the Community Climate System Model would remove the spurious southern Intertropical Convergence Zone (ITCZ) and would result in a realistically shaped South Pacific Convergence Zone (Figure 6c). Thus, ongoing work focuses on the detailed analysis of moorings with co-located wind and ocean velocity measurements (e.g. Plueddemann and Farrar 2006; Alford et al. 2012).

7. Tools and techniques

a. Microstructure database

The CPT worked in conjunction with the CLIVAR & Carbon Hydrographic Data Office (CCHDO) at Scripps Institution of Oceanography to develop a standardized format for archiving microstructure data. Data has been archived as CF-compliant NetCDF files with 1 m binned data (where possible). The database contains the following variables: time, depth, pressure, temperature, salinity, latitude, longitude, and bottom depth. The database also contains the newly designated variables: epsilon (W kg^{-1}; *ocean turbulent kinetic energy dissipation rate*), and, when available, chi-t (degree C^2 s^{-1}; *ocean dissipation rate of thermal variance from microtemperature*) and chi-c ($^{\circ}C^2$ s^{-1}; *ocean dissipation rate of thermal variance from microconductivity*). Database entries include names of the project, project PIs and cruise information (research

ship, ports of entry and exit, cruise dates, chief scientist). Database entries have project specific DOIs to cite the data in publications. Relevant cruise reports, project related papers and other documents are also contained in the data archive. At present, the database consists of 25 separate projects and can be accessed at `http://microstructure.ucsd.edu`. Newly obtained microstructure data can be uploaded to the microstructure database by sending 1-m binned data to the CCHDO office at `http://cchdo.ucsd.edu/submit`.

b. A repository for ocean mixing analysis tools, methods, and code

The availability of commercially manufactured turbulence profilers, along with an increased use of mixing proxies, have expanded the size of the mixing community and the number of publications that use mixing observations. Many variants of processing code have thus been developed in parallel by different groups. Some variants have subtle differences in methodology that can potentially lead to significant quantitative differences in the results. We thus sought to establish a community-based online repository for ”best-practices” data analysis tools used for ocean mixing and internal wave calculations. Analysis code from many independent groups is available for download from the repository, thus facilitating comparison of techniques in an open, objective way. To acccomplish this goal, a Github mixing repository was created (`https://github.com/OceanMixingCommunity/`) and populated with standard algorithms and process methods.

The goals of the public repository are to (1) enable reproducibility of analyses, (2) allow for comparison of different datasets using the same code, (3) provide a means for easy reanalysis if a bug is identified, or a best-practice change is suggested, (4) allow testing of one code against another version, and (5) provide a well-documented and version-controlled repository suitable for citation of techniques employed in publications. The code is primarily (but not exclusively) Matlab

based, and included routines for calculation of Thorpe scales, N^2, finescale parameterizations, generic and instrument-specific turbulence processing code, and sample data files.

c. Observational data analysis: the fine-scale parameterizations

Many of the insights described in this paper were inspired in part by the vast expansion of mixing data (e.g. Figure 2) that has come from widespread use of the 'finescale' parameterization for ocean mixing rates. Its increasing popularity warrants a few comments here. Finescale parameterizations produce the average dissipation rate expected over several wave periods, and therefore are helpful in assessing the spatial and temporal mean dissipation rate or diffusivity. Inferences of mixing from finescale parameterizations are more extensive than instantaneous observations of turbulence from microstructure measurements (e.g. Polzin et al. 1996; Kunze et al. 2006; Whalen et al. 2012).

Finescale parameterizations rely on the fact that the observed shear and strain variance in the thermocline and below is mainly caused by internal waves. The parameterizations also assume that the energy dissipation rate is primarily due to non-linear interactions between internal waves that transfer energy from the finescale toward smaller-scale waves that subsequently break into turbulence. As discussed in Polzin et al. (2014), an expression of the down-spectrum energy cascade in the open ocean has been developed (Henyey et al. 1986; Müller et al. 1986; Henyey and Pomphrey 1983) in terms of the shear and strain spectra. This expression allows for estimates of the dissipation rate as a function of the spectra.

Parameterizations using finescale shear and strain profiles have been tested in a variety of contexts, consistently demonstrating a factor of 2-3 agreement with microstructure inferences in open-ocean conditions (Gregg 1989; Polzin et al. 1995; Winkel et al. 2002; Polzin et al. 2014) and with strain-only inferences in a variety of locations (Wijesekera et al. 1993; Frants et al. 2013; Wa-

terman et al. 2014; Whalen et al. 2015). The shear- and strain-based parameterization is known to be less effective in regions where the underlying assumptions behind the parameterization do not apply (Polzin et al. 2014). These regions include continental shelves (Mackinnon and Gregg 2003), strong geostrophic flow regimes over rough topography (Waterman et al. 2014), and regions with very large overturning internal waves (Klymak et al. 2008). Implementation of the parameterizations in the open-ocean have revealed reasonable patterns and insight into the geography of diapycnal mixing using shear (Polzin et al. 1997; Kunze et al. 2006; Huussen et al. 2012) and strain (Kunze et al. 2006; Wu et al. 2011; Whalen et al. 2012). A global dissipation rate product that is based on both finestructure estimates and microstructure measurements is currently in preparation that will be made publicly available (C. Whalen).

d. Global internal wave models

It has only been in the last decade that global models of internal waves have been developed (Arbic et al. 2004; Simmons et al. 2004a). As described above, several global internal wave models used in the community now include atmospheric and tidal forcing, enabling examination of many issues of interest such as the global three-dimensional internal wave geography, internal wave-mesoscale interactions, and an internal gravity wave continuum spectrum that approaches the observed continuum more closely as model resolution is refined (Müller et al. 2015).

e. The Community ocean Vertical Mixing (CVMix) package

CVMix is a software package that provides transparent, robust, flexible, well-documented, and shared Fortran source codes for use in parameterizing vertical mixing processes in numerical ocean models. The project is focused on developing software for a consensus of first-order closures that return a vertical diffusivity, viscosity, and possibly a non-local transport (e.g., as in the K-Profile

Parameterization (KPP) scheme of Large et al. 1994), with each quantity dependent on the tracer or velocity being mixed. CVMix provides a software framework for the physical parameterizations arising from the internal-wave driven mixing CPT. For example, the Simmons et al. (2004b) tidal mixing scheme, available in CVMix, serves as a useful example for other tidal mixing schemes such as Melet et al. (2013a). Code development occurs within a community of scientists and engineers who make use of CVMix modules for a variety of ocean climate models (e.g., MPAS-O used at Los Alamos National Laboratory, POP used at NCAR, and MOM6 used at GFDL). CVMix modules are freely available to the community under GPLv2, using an open development approach on Github (`https://github.com/CVMix`). We solicit further contributions of parameterizations, thus enabling a very broad group of climate modelers to make use of the schemes.

8. Summary and future science directions

A frequently asked question related to this work is "Which mixing processes matter most for climate?". As with many alluringly comprehensive sounding questions, the answer is "it depends". Deep ocean mixing matters for the decadal to centennial time-scales on which the deep, global circulation evolves. The mixing process most important for the deep circulation is the one with the most power, namely the tides. The distribution of mixing above deep rough topography from nearfield tidal dissipation is the most fully developed aspect of our work, both in terms of dynamical understanding and parameterization implementation (Section 3, Figure 3). As detailed in Section 4, our understanding of farfield tidal dissipation is less complete. Lee waves may also contain significant power and play an important role in places like the Southern Ocean; preliminary results hint at a substantial role in water mass modification in this globally important region, but more observations and data-model-theory comparison is needed before we are confident of how best to represent them (Section 5, Figure 5). Non-propagating form drag is known to be important

for momentum budgets in the atmosphere, but has just begun to receive significant oceanographic attention (Trossman et al. 2016); it may be not only locally important for mixing tracers and momentum wherever strong flow encounters sharp or rough topography, but a globally important drain of mesoscale energy.

Mixing in the main pycnocline can impact heat distribution and steric sea level rise on decadal time-scales, which makes it a compelling societal problem. Turbulent mixing in this depth range is controlled by a combination of downward-propagating near-inertial waves (Section 6, Figure 6), low-mode, long-range-propagating internal tides breaking on continental slopes (Section 4, Figure 4), and by nearfield breaking of upward propagating internal tides or lee waves through nonlinear interactions. Double diffusion processes may also be significant in the main pycnocline (e.g. Schmitt et al. 2005), but are not covered here. For forward progress, a better understanding of low-mode wave breaking on slopes, with particular focus on the vertical structure of resultant dissipation (Carter and Gregg 2002; Nash et al. 2004, 2007; Martini et al. 2011; Kunze et al. 2012; Pinkel et al. 2015; Waterhouse et al. 2017), will help to constrain mixing rates.

It is increasingly clear that near-inertial wave driven mixing both below the surface boundary layer and down into the main thermocline is significantly mediated by the presence of mesoscale eddies. Areas of enhanced diffusivities have been linked to regions of elevated eddy kinetic energy, though the mechanisms are not always clear (e.g. Kunze et al. 1995; Whalen et al. 2012). In turn, interactions with internal waves may be a significant energy loss term for eddies (Buhler and McIntyre 2005; Polzin 2010; Whalen 2015; Barkan et al. 2017).

Mixing in the upper ocean matters to climate phenomena of seasonal to inter-annual, and perhaps even longer, time-scales. Turbulence beneath the surface boundary layer has a strong effect on upper ocean freshwater content and heat, and through SST changes, on a variety of coupled air-sea interactions ranging from the MJO to ENSO (e.g. Moum et al. 2016). In this depth range

(of order one hundred meters below the boundary layer), turbulence from breaking NIW plays a dominant role (Section 6, Figure 6). Again, the interaction with mesoscale eddies, and in particular mesoscale vorticity, may play a large role in setting the patterns and rates of wave propagation and dissipation in ways that are poorly constrained. We hope that continued work in this field will be closely coupled with the many active research programs focused on mixing parameterizations within the surface boundary layer, which may also be ripe for a CPT-style renovation.

Upper ocean mixing takes on a unique relevance at high latitudes. The presence of ice (either ice shelves or sea-ice) significantly changes both the dynamics and thermodynamics of turbulence near the poles, particularly in the near-surface ocean. Yet accurate representation of mixing in these environments is crucial if we are to accurately forecast everything from ice melt rates, to high latitude CO_2 absorption/outgassing, to deep water formation, to ecosystem responses to climate change. Multiple US funding agencies are increasingly putting substantial resources into process studies, long-term observations, and modeling. A formalized CPT-like framework might help bring these components together.

9. Best practices for continuing success

Once a field is in a state of readiness, where substantial observations, theory and dynamical understanding exist, the Climate Process Team structure or similar programs provide a productive template for progress. The CPT framework allows for (1) motivation to bring some parts of that research to a state of closure, (2) the opportunity to bring together observationalists, theorists and modelers to work through details of synthesizing observational reality, theoretical insights, and modeling efforts. The formal charge of CPT funding was essential to initiate this process and sustain it for the years necessary to bring such collaboration to productive fruition. A crucial component of this successful interaction has been the presence of dedicated personnel who pull

together the state of observational science and/or are embedded within modeling centers; post-docs or early career scientists fit well into this role. Similar facilitated cross-field collaborations are increasingly built into the structure of other multi-PI projects, best practices for which are well described by Cronin et al. (2009). At the same time, the epiphanies, new ideas and novel observations that fundamentally drive the field forward frequently come not from big science, but from a cornucopia of much smaller exploratory efforts and the continued small-scale development of innovative observing technology and numerical techniques. We must not lose the ability to be surprised.

Acknowledgments. We are grateful to US CLIVAR for their leadership in instigating and facilitating the Climate Process Team program, NSF and NOAA for funding, and Eric Itsweire in particular for his steadfast support and enthusiasm. We thank Alistair J. Adcroft, Mike Levy, Brandon Reichl, Todd Ringler, and Luke Van Roekel for their contributions to the CVMix project; Peter Gent; and Andreas Schmittner and David Ullman for their contributions to the advances in tidal mixing parameterizations in the CESM ocean component. NCAR is sponsored by the NSF.

References

Alford, M. H., 2001: Internal swell generation: The spatial distribution of energy flux from the wind to mixed-layer near-inertial motions. *Journal of Physical Oceanography*, **31 (8)**, 2359–2368.

Alford, M. H., 2003a: Energy available for ocean mixing redistributed through long-range propagation of internal waves. *Nature*, **423**, 159–163.

Alford, M. H., 2003b: Improved global maps and 54-year history of wind-work on ocean inertial motions. *Geophys. Res. Lett.*, **30 (8)**, 1424–1427.

Alford, M. H., 2008: Observations of parametric subharmonic instability of the diurnal internal tide in the South China Sea. *Geophys. Res. Lett.*, **35 (L15602)**, doi:10.1029/2008GL034 720.

Alford, M. H., M. F. Cronin, and J. M. Klymak, 2012: Annual Cycle and Depth Penetration of Wind-Generated Near-Inertial Internal Waves at Ocean Station Papa in the Northeast Pacific. *Journal of Physical Oceanography*, **42 (6)**, 889–909.

Alford, M. H., J. B. Girton, G. Voet, G. S. Carter, J. B. Mickett, and J. M. Klymak, 2013: Turbulent mixing and hydraulic control of abyssal water in the Samoan Passage. *Geophys. Res. Lett.*, **40 (17)**, 4668–4674.

Alford, M. H., J. M. Klymak, and G. S. Carter, 2014: Breaking internal lee waves at Kaena Ridge, Hawaii. *Geophys. Res. Lett.*, **41**, 906–912.

Alford, M. H., J. A. MacKinnon, H. L. Simmons, and J. D. Nash, 2016: Near-inertial internal gravity waves in the ocean. *Annual review of marine science*, **8**, 95–123.

Alford, M. H., J. A. MacKinnon, Z. Zhao, R. Pinkel, J. Klymak, and T. Peacock, 2007: Internal waves across the Pacific. *Geophys. Res. Lett.*, **34 (L24601)**, doi:10.1029/2007GL031 566.

Alford, M. H., and M. Whitmont, 2007: Seasonal and spatial variability of near-inertial kinetic energy from historical moored velocity records. *Journal of Physical Oceanography*, **37 (8)**, 2022–2037.

Alford, M. H., and Coauthors, 2015: The formation and fate of internal waves in the South China Sea. *Nature*, **521**, DOI:10.1038/nature14 399.

Ansong, J. K., B. K. Arbic, M. C. Buijsman, J. G. Richman, J. F. Shriver, and A. J. Wallcraft, 2015: Indirect evidence for substantial damping of low-mode internal tides in the open ocean. *Journal of Geophysical Research: Oceans*, **120 (9)**, 6057–6071.

Ansong, J. K., and Coauthors, 2017: Semidiurnal internal tide energy fluxes and their variability in a global ocean model and moored observations. *Journal of Geophysical Research: Oceans*, n/a–n/a, doi:10.1002/2016JC012184, URL http://dx.doi.org/10.1002/2016JC012184.

Arbic, B. K., S. T. Garner, R. Hallberg, and H. L. Simmons, 2004: The accuracy of surface elevations in forward global barotropic and baroclinic tide models. *Deep Sea Research Part II*, **51**, 3069–3101.

Arbic, B. K., A. J. Wallcraft, and E. J. Metzger, 2010: Concurrent simulation of the eddying general circulation and tides in a global ocean model. *Ocean Modelling*, **32 (3)**, 175–187.

Balmforth, N. J., and T. Peacock, 2009: Tidal conversion by supercritical topography. *Journal of Physical Oceanography*, **39**, 1965–1974.

Barkan, R., K. B. Winters, and J. C. McWilliams, 2017: Stimulated imbalance and the enhancement of eddy kinetic energy dissipation by internal waves. *Journal of Physical Oceanography*, **47 (1)**, 181–198.

Bell, T., 1975: Topographically generated internal waves in the open ocean. *Journal of Geophysical Research*, **80**, 320–327.

Bretherton, F. P., 1969: Momentum transport by gravity waves. *Quarterly Journal of the Royal Meteorological Societyuarterly journal of the royal meteorological society*, **95 (404)**, 213–243.

Bryan, K., and L. J. Lewis, 1979: A water mass model of the world ocean. *Journal of Geophysical Research*, **84**, 2503–2517.

Buhler, O., and M. Holmes-Cerfon, 2011: Decay of an internal tide due to random topography in the ocean. *J. Fluid Mech*, **678**, 271–293– doi:10.1017–jfm.2011.115.

Buhler, O., and M. McIntyre, 2005: Wave capture and wave-vortex duality. *Journal of Fluid Mechanics*, **534**, 67–96.

Buijsman, M., S. Legg, and J. Klymak, 2012: Double ridge internal tide interference and its effect on dissipation in Luzon Strait. *Journal of Physical Oceanography*, **42**, 1337–1356.

Buijsman, M. C., and Coauthors, 2014: Three-Dimensional Double-Ridge Internal Tide Resonance in Luzon Strait. *Journal of Physical Oceanography*, **44**, DOI:10.1175/JPO–D–13–024.1.

Buijsman, M. C., and Coauthors, 2016: Impact of internal wave drag on the semidiurnal energy balance in a global ocean circulation model. *Journal of Physical Oceanography*, **46**, 1399–1419, doi:10.1175/JPO-D-15-0074.1.

Cacchione, D., and C. Wunsch, 1974: Experimental study of internal waves over a slope. *Journal of Fluid Mechanics*, **66**, 223–239.

Carter, G. S., and M. C. Gregg, 2002: Intense, variable mixing near the head of Monterey Submarine Canyon. *Journal of Physical Oceanography*, **32**, 3145–3165.

Clement, L., E. Frajka-Williams, K. L. Sheen, J. A. Brearley, and A. C. Naveira Garabato, 2016: Generation of internal waves by eddies impinging on the western boundary of the North Atlantic. *Journal of Physical Oceanography*, **46**, 1067–1079.

Cronin, M. F., S. Legg, and P. Zuidema, 2009: Climate research: Best practices for process studies. *Bulletin of the American Meteorological Society*, **90 (7)**, 917–918.

Cusack, J. M., A. C. Garabato, D. A. Smeed, and J. B. Girton, 2017: Observation of a large lee wave in the drake passage. *Journal of Physical Oceanography*, **in press (0)**, null, doi:10.1175/JPO-D-16-0153.1.

Danabasoglu, G., S. Bates, B. Briegleb, S. Jayne, M. Jochum, W. Large, S. Peacock, and S. Yeager, 2012: The CCSM4 ocean component. *Journal of Climate*, **25**, 1361–1389.

Danabasoglu, G., W. Large, and B. Briegleb, 2010: Climate impacts of parameterized nordic sea overflows. *Journal of Geophysical Research*, **115, C11005**, doi:10.1029/2010JC006243.

D'Asaro, E., 1985: The energy flux from the wind to near-inertial motions in the mixed layer. *Journal of Physical Oceanography*, **15**, 943–959.

D'Asaro, E. A., C. E. Eriksen, M. D. Levine, P. Niiler, C. A. Paulson, and P. V. Meurs, 1995: Upper-ocean inertial currents forced by a strong storm, part I, Data and comparisons with linear theory. *Journal of Physical Oceanography*, **25**, 2909–2936.

De Lavergne, C., G. Madec, J. Le Sommer, A. G. Nurser, and A. C. Naveira Garabato, 2016: The impact of a variable mixing efficiency on the abyssal overturning. *Journal of Physical Oceanography*, **46 (2)**, 663–681.

Decloedt, T., and D. Luther, 2010: On a simple empirical parameterization of topography-catalyzed diapycnal mixing in the abyssal ocean. *Journal of Physical Oceanography*, **40 (3)**, 487–508.

Dohan, K., and R. E. Davis, 2011: Mixing in the transition layer during two storm events. *Journal of Physical Oceanography*, **41 (1)**, 42–66.

Dossmann, Y., M. G Rosevear, R. W. Griffiths, G. O. Hughes, M. Copeland, and Coauthors, 2016: Experiments with mixing in stratified flow over a topographic ridge. *Journal of Geophysical Research: Oceans*, **121 (9)**, 6961–6977.

Dunne, J. P., and Coauthors, 2012: GFDL's ESM2 global coupled climate-carbon Earth System Models Part I: Physical formulation and baseline simulation characteristics. *Journal of Climate*, **25**, 6646—6665.

Dunphy, M., and K. G. Lamb, 2014: Focusing and vertical mode scattering of the first mode internal tide by mesoscale eddy interaction. *J. Geophys. Res. Oceans*, **119**, doi:doi:10.1002/2013JC009293.

Dushaw, B., B. Howe, B. Cornuelle, P. Worcester, and D. Luther, 1995: Barotropic and baroclinic tides in the central North Pacific Ocean determined from long-range reciprocal acoustic transmissions. *Journal of Physical Oceanography*, **25**, 631–647.

Eden, C., and D. Olbers, 2014: An energy compartment model for propagation, non-linear interaction and dissipation of internal gravity waves. *Journal of Physical Oceanography*, **44**, 2093–2106, doi:10.1175/JPO-D-13-0224.1.

Egbert, G. D., and R. D. Ray, 2003: Semi-diurnal and diurnal tidal dissipation from TOPEX/Poseidon altimetry. *Geophys. Res. Lett.*, **30**, 1907, doi:10.1029/2003GL017676, URL http://dx.doi.org/10.1029/2003GL017676.

Ferrari, R., and C. Wunsch, 2009: Ocean circulation kinetic energy: Reservoirs, sources, and sinks. *Annual Review of Fluid Mechanics*, **41 (1)**, 253–282, doi:10.1146/annurev.fluid.40.111406.102139.

Ferron, B. H., H. Mercier, K. Speer, A. Gargett, and K. Polzin, 1998: Mixing in the Romanche Fracture Zone. *Journal of Physical Oceanography*, **28**, 1929–1945.

Frants, M., G. M. Damerell, S. T. Gille, K. J. Heywood, J. A. Mackinnon, and J. Sprintall, 2013: An Assessment of Density-Based Finescale Methods for Estimating Diapycnal Diffusivity in the Southern Ocean. *Journal of Atmospheric and Oceanic Technology*, **30 (11)**, 2647–2661.

Friedrich, T., A. Timmermann, T. Decloedt, D. S. Luther, and A. Mouchet, 2011: The effect of topography-enhanced diapycnal mixing on ocean and atmospheric circulation and marine biogeochemistry. *Ocean Modelling*, **39**, 262–274.

Furuichi, N., T. Hibiya, and Y. Niwa, 2008: Model predicted distribution of wind-induced internal wave energy in the world's oceans. *J. Geophys. Res.*, **113 (C09034)**, doi:10.1029/2008JC004768.

Gargett, A. E., 1984: Vertical eddy diffusivity in the ocean interior. *Journal of Marine Research*, **42**, 359–393.

Garner, S. T., 2005: A topographic drag closure built on an analytical base flux. *Journal of Atmospheric Science*, **62**, 2302–2315.

Garrett, C., and E. Kunze, 2007: Internal tide generation in the deep ocean. *Annual Review of Fluid Mechanics*, **39**, 57–87.

Gaspar, P., Y. Gregoris, and J. Lefevre, 1990: A simple eddy kinetic energy model for simulations of the oceanic vertical mixing: Tests at station Papa and long-term upper ocean study site. *Journal of Geophysical Research*, **95**, 16 179–16 193.

Green, J. A. M., and J. Nycander, 2013: A comparison of tidal conversion parameterizations for tidal models. *Journal of Physical Oceanography*, **43**, 104–119.

Gregg, M., 1989: Scaling turbulent dissipation in the thermocline. *J. Geophys. Res.*, **94 (C7)**, 9686–9698.

Gregg, M. G., E. A. D'Asaro, and J. J. Riley, 2017: Mixing coefficients and mixing efficiency in the ocean. *Annual Reviews of Marine Science*, **(in press)**.

Griffies, S. M., R. C. Pacanowski, and R. W. Hallberg, 2000: Spurious diapycnal mixing associated with advection in a z-coordinate ocean model. *Monthely Weather Review*, **128**, 538–564.

Hall, R., J. Huthnance, and R. Williams, 2013: Internal wave reflection on shelf-slopes with depth-varying stratification. *Journal of Physical Oceanography*, **43**, 243–258.

Harrison, M., and R. Hallberg, 2008: Pacific subtropical cell response to reduced equatorial dissipation. *Journal of Physical Oceanography*, **38**, 1894–1912.

Hazewinkel, J., and K. B. Winters, 2011: PSI of the internal tide on a β-plane: Flux divergence and near-inertial wave propagation. *Journal of Physical Oceanography*, **41**, 1673–1682.

Helfrich, K. R., and R. H. J. Grimshaw, 2008: Nonlinear disintegration of the internal tide. *Journal of Physical Oceanography*, **38**, 686–701.

Henyey, F., and N. Pomphrey, 1983: Eikonal description of internal wave interactions: A non-diffusive picture of "induced diffusion". *Dynamics of Atmospheres and Oceans*, **7**, 189–219.

Henyey, F. S., J. Wright, and S. M. Flatté, 1986: Energy and action flow through the internal wave field. *J. Geophys. Res.*, **91 (C7)**, 8487–8495.

Huussen, T. N., A. C. Naveira-Garabato, H. L. Bryden, and E. L. McDonagh, 2012: Is the deep Indian Ocean MOC sustained by breaking internal waves? *J. Geophys. Res.*, **117 (C8)**, C08 024.

Ilıcak, M., A. Adcroft, S. Griffies, and R. Hallberg, 2012: Spurious dianeutral mixing and the role of momentum closure. *Ocean Modelling*, **45–46**, 37–58.

Ivey, G., and R. Nokes, 1989: Vertical mixing due to the breaking of critical internal waves on sloping boundaries. *Journal of Fluid Mechanics*, **204**, 479–500.

Ivey, G., K. Winters, and I. de Silva, 2000: Turbulent mixing in a sloping benthic boundary layer energized by internal waves. *Journal of Fluid Mechanics*, **418**, 59–76.

Ivey, G., K. Winters, and J. Koseff, 2008: Density stratification, turbulence, but how much mixing? *Ann. Rev. Fluid Mech.*, **40**, 169–184.

Jackson, L., R. Hallberg, and S. Legg, 2008: A Parameterization of Shear-Driven Turbulence for Ocean Climate Models. *Journal of Physical Oceanography*, **38**, 1033–1053.

Jayne, S. R., 2009: The impact of abyssal mixing parameterizations in an ocean general circulation model. *Journal of Physical Oceanography*, **39**, 1756—1775.

Jayne, S. R., and L. C. St. Laurent, 2001: Parameterizing tidal dissipation over rough topography. *Geophys. Res. Lett.*, **28 (5)**, 811–814.

Jochum, M., 2009: Impact of latitudinal variations in vertical diffusivity on climate simulations. *Journal of Geophysical Research*, **114, C01010**, doi:10.1029/2008JC005030.

Jochum, M., B. P. Briegleb, G. Danabasoglu, W. G. Large, N. J. Norton, S. R. Jayne, M. H. Alford, and F. O. Bryan, 2013: The impact of oceanic near-inertial waves on climate. *J. Climate*, **26 (9)**, 2833–2844, doi:10.1175/JCLI-D-12-00181.1.

Johnston, T. M. S., and M. A. Merrifield, 2003: Internal tide scattering at seamounts, ridges and islands. *Journal of Geophysical Research*, **108(C6)**, doi:10.1029/2002JC001528.

Johnston, T. M. S., D. L. Rudnick, and S. M. Kelly, 2015: Standing internal tides in the Tasman Sea observed by gliders. *Journal of Physical Oceanography*, **45**, doi:10.1175/JPO-D-15-0038.1.

Kelly, S. M., N. L. Jones, J. D. Nash, and A. F. Waterhouse, 2013: The geography of semidiurnal mode-1 internal-tide energy loss. *Geophysical Research Letters*, **40**, 4689–4693, doi:10.1002/grl.50872.

Kelly, S. M., J. D. Nash, K. I. Martini, M. H. Alford, and E. Kunze, 2012: The cascade of tidal energy from low to high modes on a continental slope. *Journal of Physical Oceanography*, **42**, doi:10.1175/JPO-11-0231.1.

Kerry, C., B. Powell, and G. Carter, 2014: The impact of subtidal circulation on internal-tide-induced mixing in the Philippine sea. *Journal of Physical Oceanography*, **44**, 3209–3224, doi:10.1175/JPO-D-13-0142.1.

Klinger, B. A., J. Marshall, and U. Send, 1996: Representation of convective plumes by vertical adjustment. *Journal of Geophysical Research*, **101**, 18 175–18 182.

Klymak, J., M. Buijsman, S. Legg, and R. Pinkel, 2013: Parameterizing surface and internal tide scattering and breaking on supercritical topography: the one- and two-ridge cases. *Journal of Physical Oceanography*, **43**, 1380–1397.

Klymak, J. M., M. H. Alford, R. Pinkel, R. C. Lien, and Y. J. Yang, 2011: The breaking and scattering of the internal tide on a continental slope. *Journal of Physical Oceanography*, **41 (5)**, 926–945, doi:10.1175/2010JPO4500.1.

Klymak, J. M., S. Legg, and R. Pinkel, 2010: A simple parameterization of turbulent tidal mixing near supercritical topography. *Journal of Physical Oceanography*, **40 (9)**, 2059–2074, doi:10.1175/2010JPO4396.1, http://journals.ametsoc.org/doi/pdf/10.1175/2010JPO4396.1.

Klymak, J. M., R. Pinkel, and L. Rainville, 2008: Direct breaking of the internal tide near topography: Kaena Ridge, Hawaii. *Journal of Physical Oceanography*, **38**, 380–399.

Klymak, J. M., and Coauthors, 2006: An estimate of tidal energy lost to turbulence at the Hawaiian Ridge. *Journal of Physical Oceanography*, **36 (6)**, 1148–1164.

Kunze, E., 2017: Internal-wave-driven mixing: Geography and budgets. *J. Phys. Oceanogr.*, **(in review)**.

Kunze, E., E. Firing, J. Hummon, T. K. Chereskin, and A. Thurnherr, 2006: Global abyssal mixing inferred from lowered ADCP shear and CTD strain profiles. *Journal of Physical Oceanography*, **36**, 1553–1576.

Kunze, E., C. MacKay, E. E. McPhee-Shaw, K. Morrice, J. B. Girton, and S. R. Terker, 2012: Turbulent mixing and exchange with interior waters on sloping boundaries. *Journal of Physical Oceanography*, **42**, 910–927.

Kunze, E., R. W. Schmitt, and J. M. Toole, 1995: The energy balance in a warm-core ring's near-inertial critical layer. *Journal of Physical Oceanography*, **25 (5)**, 942–957.

Large, W., and G. Crawford, 1995: Observations and simulations of upper-ocean response to wind events during the ocean storms experiment. *Journal of physical Oceanography*, **25 (11)**, 2831–2852.

Large, W., J. McWilliams, and S. Doney, 1994: Oceanic vertical mixing: a review and a model with a nonlocal boundary layer parameterization. *Reviews of Geophysics*, **32**, 363–403.

Lefauve, A., C. Muller, and A. Melet, 2015: A three-dimensional map of tidal dissipation over abyssal hills. *Journal of Geophysical Research: Oceans*, **120 (7)**, 4760–4777.

Legg, S., 2014: Scattering of low-mode internal waves at finite isolated topography. *Journal of Physical Oceanography*, **44 (1)**, 359–383, doi:10.1175/JPO-D-12-0241.1.

Legg, S., and A. Adcroft, 2003: Internal wave breaking at concave and convex continental slopes. *Journal of Physical Oceanography*, **33**, 2224–2246.

Legg, S., R. Hallberg, and J. Girton, 2006: Comparison of entrainment in overflows simulated by z-coordinate, isopycnal and non-hydrostatic models. *Ocean Modelling*, **11**, 69–97.

Legg, S., and J. M. Klymak, 2008: Internal hydraulic jumps and overturning generated by tidal flow over a steep ridge. *Journal of Physical Oceanography*, **38**, 1949–1964.

Lighthill, J., 1976: *Waves in fluids*. Cambridge University Press.

Llewellyn Smith, S. G., and W. R. Young, 2003: Tidal conversion at a very steep ridge. *J. Fluid Mech.*, **495**, 175–191.

Lumpkin, R., and K. Speer, 2007: Global ocean meridional overturning. *Journal of Physical Oceanography*, **37**, 2550–2562.

Lvov, Y., K. L. Polzin, and E. G. Tabak, 2004: Energy spectra of the ocean's internal wave field: Theory and observations. *Phys. Rev. Lett.*, **92 (12)**, 128 501–1–128 501–4.

MacKinnon, J., 2013: Mountain waves in the deep ocean. *Nature*, **501 (7467)**, 321–322.

MacKinnon, J., Louis St. Laurent, and A. N. Garabato, 2013a: Diapycnal mixing processes in the ocean interior. *Ocean Circulation and Climate, 2nd Edition: A 21st century perspective*, G. Siedler, S. M. Griffies, J. Gould, and J. Church, Eds., International Geophysics Series, Vol. 103, Academic Press, 159–183.

MacKinnon, J., and K. Winters, 2003: Spectral evolution of bottom-forced internal waves. *Near-Boundary Processes and Their Parameterization, Proceedings of the 13th 'Aha Huliko'a Hawaiian Winter Workshop*, P. Muller, and D. Henderson, Eds., 73–83.

MacKinnon, J., and K. Winters, 2005: Subtropical catastrophe: significant loss of low-mode tidal energy at 28.9. *Geophys. Res. Lett.*, **32**, 1–5.

MacKinnon, J. A., M. H. Alford, R. Pinkel, J. Klymak, and Z. Zhao, 2013b: The latitudinal dependence of shear and mixing in the Pacific transiting the critical latitude for PSI. *Journal of Physical Oceanography*, **43 (1)**, 3–16.

MacKinnon, J. A., M. H. Alford, O. Sun, R. Pinkel, Z. Zhao, and J. Klymak, 2013c: Parametric subharmonic instability of the internal tide at 29N. *Journal of Physical Oceanography*, **43**, 17–28, doi:10.1175/JPO-D-11-0108.1.

Mackinnon, J. A., and M. C. Gregg, 2003: Shear and Baroclinic Energy Flux on the Summer New England Shelf. *Journal of Physical Oceanography*, **33**, 1462–1475.

Martini, K. I., M. H. Alford, E. Kunze, S. M. Kelly, and J. D. Nash, 2011: Observations of internal tides on the Oregon continental slope. *Journal of Physical Oceanography*, **41**, 1772–1794.

Martini, K. I., M. H. Alford, E. Kunze, S. M. Kelly, and J. D. Nash, 2013: Internal Bores and Breaking Internal Tides on the Oregon Continental Slope. *Journal of Physical Oceanography*, **43 (1)**, 120–139.

Mashayek, A., C. Caulfield, and W. Peltier, 2013: Time-dependent, non-monotonic mixing in stratified turbulent shear flows: implications for oceanographic estimates of buoyancy flux. *Journal of Fluid Mechanics*, **736**, 570–593.

Mathur, M., G. S. Carter, and T. Peacock, 2014: Topographic scattering of the low-mode internal tide in the deep ocean. *Journal of Geophysical Research: Oceans*, **119**, 2165–2182, doi:10.1002/2013JC009152.

McComas, C. H., 1977: Equilibrium mechanisms within the oceanic internal wave field. *Journal of Physical Oceanography*, **7**, 836–845.

Melet, A., R. Hallberg, A. Adcroft, M. Nikurashin, and S. Legg, 2015: Energy flux into internal lee waves: sensitivity to future climate changes using linear theory and a climate model. *Journal of Climate*, **28**, 2365–2384.

Melet, A., R. Hallberg, S. Legg, and M. Nikurashin, 2014: Sensitivity of the ocean state to lee wave–driven mixing. *Journal of Physical Oceanography*, **44 (3)**, 900–921, doi:10.1175/JPO-D-13-072.1.

Melet, A., R. Hallberg, S. Legg, and K. L. Polzin, 2013a: Sensitivity of the ocean state to the vertical distribution of internal-tide-driven mixing. *Journal of Physical Oceanography*, **43 (3)**, 602–615, doi:http://dx.doi.org/10.1175/JPO-D-12-055.1.

Melet, A., S. Legg, and R. Hallberg, 2016: Climatic impacts of parameterized local and remote tidal mixing. *Journal of Climate*, **29 (10)**, 3473–3500.

Melet, A., M. Nikurashin, C. J. Muller, S. Falahat, J. Nycander, P. G. Timko, B. K. Arbic, and J. A. Goff, 2013b: Internal tide generation by abyssal hills using analytical theory. *Journal of Geophysical Research - Oceans*, **118**, 6303–6318.

Moum, J. N., K. Pujiana, R.-C. Lien, and W. D. Smyth, 2016: Ocean feedback to pulses of the madden–julian oscillation in the equatorial indian ocean. *Nature communications*, **7**.

Muller, C. J., and O. Bühler, 2009: Saturation of the internal tides and induced mixing in the abyssal ocean. *Journal of Physical Oceanography*, **39**, 2077–2096.

Müller, M., B. K. Arbic, J. G. Richman, J. F. Shriver, E. L. Kunze, R. B. Scott, A. J. Wallcraft, and L. Zamudio, 2015: Toward an internal gravity wave spectrum in global ocean models. *Geophysical Research Letters*, **42 (9)**, 3474–3481.

Müller, M., J. Cherniawsky, M. Foreman, and J.-S. von Storch, 2012: Global map of M_2 internal tide and its seasonal variability from high resolution ocean circulation and tide modelling. *Geophysical Research Letters*, **39**, L19607, doi:10.1029/2012GL053320.

Müller, P., G. Holloway, F. Henyey, and N. Pomphrey, 1986: Nonlinear interactions among internal gravity waves. *Rev. Geophys*, **24 (3)**, 493–536.

Müller, P., and A. Natarov, 2003: The internal wave action model (iwam). *Near-Boundary Processes and Their Parameterization: Proc.'Aha Huliko'a Winter Workshop*, Citeseer, 95–105.

Musgrave, R., R. Pinkel, J. MacKinnon, M. R. Mazloff, and W. Young, 2016: Stratified tidal flow over a tall ridge above and below the turning latitude. *Journal of Fluid Mechanics*, **793**, 933–957.

Nagai, T., and T. Hibiya, 2015: Internal tides and associated vertical mixing in the indonesian archipelago. *Journal of Geophysical Research: Oceans*, **120 (5)**, 3373–3390.

Nash, J. D., M. H. Alford, E. Kunze, K. I. Martini, and S. Kelly, 2007: Hotspots of deep ocean mixing on the Oregon continental slope. *Geophys. Res. Lett.*, **34 (L01605)**, doi:10.1029/2006GL028 170.

Nash, J. D., E. Kunze, J. M. Toole, and R. W. Schmitt, 2004: Internal tide reflection and turbulent mixing on the continental slope. *Journal of Physical Oceanography*, **34**, 1117–1134.

Naveira Garabato, A. C., K. L. Polzin, B. A. King, K. J. Heywood, and M. Visbeck, 2004: Widespread intense turbulent mixing in the Southern Ocean. *Science*, **303**, 210–213.

Nikurashin, M., and R. Ferrari, 2011: Global energy conversion rate from geostrophic flows into internal lee waves in the deep ocean. *Geophys. Res. Lett.*, **38 (L08610)**, doi:10.1029/2011GL046 576.

Nikurashin, M., and R. Ferrari, 2013: Overturning circulation driven by breaking internal waves in the deep ocean. *Geophys. Res. Lett.*, **40 (12)**, 3133–3137, doi:10.1002/grl.50542.

Nikurashin, M., R. Ferrari, N. Grisouard, and K. Polzin, 2014: The impact of finite amplitude bottom topography on internal wave generation in the Southern Ocean. *Journal of Physical Oceanography*, **44**, 2938–2950.

Nikurashin, M., and S. Legg, 2011: A mechanism for local dissipation of internal tides generated at rough topography. *Journal of Physical Oceanography*, **41**, 378–395.

Niwa, Y., and T. Hibiya, 2011: Estimation of baroclinic tide energy available for deep ocean mixing based on three-dimensional global numerical simulations. *Journal of Oceanography*, **67 (4)**, 493–502.

Niwa, Y., and T. Hibiya, 2014: Generation of baroclinic tide energy in a global three-dimensional numerical model with different spatial grid resolutions. *Ocean Modelling*, **80**, 59–73.

Osborn, T. R., 1980: Estimates of the local rate of vertical diffusion from dissipation measurements. *Journal of Physical Oceanography*, **10**, 83–89.

Pacanowski, R. C., and G. Philander, 1981: Parameterization of vertical mixing in numerical models of the tropical ocean. *Journal of Physical Oceanography*, **11**, 1442–1451.

Palmer, W. R., G. J. Shutts, and R. Swinbank, 1986: Alleviation of systematic westerly bias in general circulation and numerical weather prediction models through an orographic gravity

wave drag parameterization. *Quarterly Journal of the Royal Meteorological Society*, **112(474)**, 1001–1039.

Peltier, W. R., and C. P. Caulfield, 2003: Mixing efficiency in stratified shear flows. *Annual Review of Fluid Mechanics*, **35 (1)**, 135–167, doi:10.1146/annurev.fluid.35.101101.161144.

Pierrehumbert, R., and J. Bacmeister, 1987: On the realizability of long's model solutions for nonlinear stratified flow over an obstacle. *Stratified Flows*, ASCE, 99–112.

Pinkel, R., and Coauthors, 2015: Breaking internal tides keep the ocean in balance. *EOS Transactions*, **96**.

Plueddemann, A. J., and J. T. Farrar, 2006: Observations and models of the energy flux from the wind to mixed layer inertial currents. *Deep-Sea Research*, **53**, 5–30.

Polzin, K. L., 2004a: A flux representation of internal wave spectral transports. *Journal of Physical Oceanography*, **34**, 214–230.

Polzin, K. L., 2004b: Idealized solutions for the energy balance of the finescale internal wave field. *Journal of Physical Oceanography*, **34 (1)**, 231–246.

Polzin, K. L., 2009: An abyssal recipe. *Ocean Modelling*, **30**, 298–309.

Polzin, K. L., 2010: Mesoscale Eddy-Internal Wave Coupling. Part II: Energetics and Results from PolyMode. *Journal of Physical Oceanography*, **40 (4)**, 789–801.

Polzin, K. L., A. C. Naveira Garabato, T. N. Huussen, B. M. Sloyan, and S. Waterman, 2014: Finescale parameterizations of turbulent dissipation. *Journal of Geophysical Research: Oceans*, **119 (2)**, 1383–1419.

Polzin, K. L., N. S. Oakey, J. M. Toole, and R. W. Schmitt, 1996: Fine structure and microstructure characteristics across the northwest Atlantic Subtropical Front. *J. Geophys. Res.*, **101 (C6)**, 14 111–14 121.

Polzin, K. L., J. M. Toole, J. R. Ledwell, and R. W. Schmitt, 1997: Spatial variability of turbulent mixing in the abyssal ocean. *Science*, **276**, 93–96.

Polzin, K. L., J. M. Toole, and R. W. Schmitt, 1995: Finescale parameterizations of turbulent dissipation. *Journal of Physical Oceanography*, **25**, 306–328.

Rahmstorf, S., 1993: A fast and complete convection scheme for ocean models. *Ocean Modelling*, **101**, 9–11.

Rainville, L., and R. Pinkel, 2006: Baroclinic energy flux at the Hawaiian Ridge: Observations from the R/P FLIP. *Journal of Physical Oceanography*, **36 (6)**, 1104–1122.

Ray, R. D., and G. T. Mitchum, 1996: Surface manifestation of internal tides generated near Hawaii. *Geophys. Res. Lett.*, **23 (16)**, 2101–2104.

Rimac, A., J.-S. v. Storch, and C. Eden, 2016: The total energy flux leaving the ocean's mixed layer. *Journal of Physical Oceanography*, **46 (6)**, 1885–1900.

Rimac, A., J.-S. von Storch, C. Eden, and H. Haak, 2013: The influence of high-resolution wind stress field on the power input to near-inertial motions in the ocean. *Geophysical Research Letters*, **40 (18)**, 4882–4886, doi:10.1002/grl.50929.

Rocha, C. B., T. K. Chereskin, S. T. Gille, and D. Menemenlis, 2016: Mesoscale to submesoscale wavenumber spectra in drake passage. *Journal of Physical Oceanography*, **46 (2)**, 601–620, doi:10.1175/JPO-D-15-0087.1.

Rudnick, D., and Coauthors, 2003: From tides to mixing along the Hawaiian Ridge. *Science*, **301**, 355–357.

Salehipour, H., W. R. Peltier, C. B. Whalen, and J. A. Mackinnon, 2016: A new characterization of the turbulent diapycnal diffusivities of mass and momentum in the ocean. *Geophysical Research Letters*, n/a–n/a.

Schmitt, R. W., J. R. Ledwell, E. T. Montgomery, K. L. Polzin, and J. M. Toole, 2005: Enhanced diapycnal mixing by salt fingers in the thermocline of the tropical Atlantic. *Science*, **308**, 685–688.

Schmittner, A., and G. Egbert, 2014: An improved parameterization of tidal mixing for ocean models. *Geosci. Model Dev.*, **7**, 211–224.

Scott, R., J. Goff, A. Garabato, and A. Nurser, 2011: Global rate and spectral characteristics of internal gravity wave generation by geostrophic flow over topography. *Journal of Geophysical Research*, **116 (C9)**, C09 029.

Sheen, K., and Coauthors, 2014: Eddy-induced variability in southern ocean abyssal mixing on climatic timescales. *Nature Geoscience*, **7(8)**, 577–582.

Sheen, K. L., and Coauthors, 2013: Rates and mechanisms of turbulent dissipation and mixing in the Southern Ocean: Results from the Diapycnal and Isopycnal Mixing Experiment in the Southern Ocean (DIMES). *J. Geophys. Res.*, **118**, 1–19, doi:http://10.1002/jgrc.20217.

Shriver, J., B. K. Arbic, J. Richman, R. Ray, E. Metzger, A. Wallcraft, and P. Timko, 2012: An evaluation of the barotropic and internal tides in a high-resolution global ocean circulation model. *Journal of Geophysical Research: Oceans (1978–2012)*, **117 (C10)**.

Shriver, J., J. Richman, and B. Arbic, 2014: How stationary are the internal tides in a high-resolution global ocean circulation model? *Journal of Geophysical Research: Oceans*, **119**, 2769–2787, doi:10.1002/2013JC009423.

Silverthorne, K. E., and J. M. Toole, 2009: Seasonal kinetic energy variability of near-inertial motions. *Journal of Physical Oceanography*, **39 (4)**, 1035–1049.

Simmons, H. L., 2008: Spectral modification and geographic redistribution of the semi-diurnal internal tide. *Ocean Modelling*, **21**, 126–138.

Simmons, H. L., and M. H. Alford, 2012: Simulating the long range swell of internal waves generated by ocean storms. *Oceanography*, **25 (2)**, 30–41.

Simmons, H. L., R. W. Hallberg, and B. K. Arbic, 2004a: Internal wave generation in a global baroclinic tide model. *Deep-Sea Res II*, **51**, 3043–3068.

Simmons, H. L., S. R. Jayne, L. C. St.Laurent, and A. J. Weaver, 2004b: Tidally driven mixing in a numerical model of the ocean general circulation. *Ocean Modelling*, **6**, 245–263.

Slinn, D. N., and J. J. Riley, 1996: Turbulent mixing in the oceanic boundary layer caused by internal wave reflection from sloping terrain. *Dynamics of atmospheres and oceans*, **24 (1)**, 51–62.

St. Laurent, L., and C. Garrett, 2002: The role of internal tides in mixing the deep ocean. *Journal of Physical Oceanography*, **32 (10)**, 2882–2899.

St. Laurent, L., H. Simmons, and S. Jayne, 2002: Estimating tidally driven mixing in the deep ocean. *Geophys. Res. Lett.*, **29 (23)**.

St. Laurent, L. C., 2008: Turbulent dissipation on the margins of the South China Sea. *Geophys. Res. Lett.*, **35 (L23615)**, doi:10.1029/2008GL035 520.

St. Laurent, L. C., and J. D. Nash, 2004: An examination of the radiative and dissipative properties of deep ocean internal tides. *Deep-Sea Research II*, **51**, 3029–3042.

St. Laurent, L. C., A. C. Naveira Garabato, J. R. Ledwell, A. M. Thurnherr, J. M. Toole, and A. J. Watson, 2012: Turbulence and diapycnal mixing in Drake Passage. *Journal of Physical Oceanography*, **42**, 2143–2152.

St. Laurent, L. C., and H. L. Simmons, 2006: Estimates of power consumed by mixing in the ocean interior. *Journal of Climate*, **19**, 4877–4890.

Staquet, C., and J. Sommeria, 2002: Internal gravity waves: From instability to turbulence. *Annual Reviews of Fluid Mechanics*, **34**, 559–593.

Sun, O. M., and R. Pinkel, 2012: Energy transfer from high-shear, low-frequency internal waves to high-frequency waves near Kaena Ridge, Hawai'i. *Journal of Physical Oceanography*, **42**, doi:10.1175/JPO-D-11-0117.1.

Sun, O. M., and R. Pinkel, 2013: Subharmonic energy transfer from the semidiurnal internal tide to near-diurnal motions over Kaena Ridge, Hawai'i. *Journal of Physical Oceanography*, doi: 10.1175/JPO-D-12-0141.1.

Tanaka, T., I. Yasuda, Y. Tanaka, and G. S. Carter, 2013: Numerical study on tidal mixing along the shelf break in the Green Belt in the southeastern Bering Sea. *Journal of Geophysical Research: Oceans*, **118**, 6525–6542.

Thoppil, P., J. Richman, and P. Hogan, 2011: Energetics of a global ocean circulation model compared to observations. *Geophysical Research Letters*, **38**, L15 607.

Thurnherr, A. M., L. C. St. Laurent, K. G. Speer, J. M. Toole, and J. R. Ledwell, 2005: Mixing associated with sills in a canyon on the midocean ridge flank. *Journal of Physical Oceanography*, **35**, 1370–1381.

Trossman, D. S., B. K. Arbic, S. T. Garner, J. A. Goff, S. R. Jayne, E. J. Metzger, and A. J. Wallcraft, 2013: Impact of parameterized lee wave drag on the energy budget of an eddying global ocean model. *Ocean Modelling*, **72**, 119–142.

Trossman, D. S., B. K. Arbic, J. G. Richman, S. T. Garner, S. R. Jayne, and A. J. Wallcraft, 2016: Impact of Topographic Internal Lee Wave Drag on an Eddying Global Ocean Model. *Ocean Modelling*, **97**, 109–128.

Trossman, D. S., S. Waterman, K. L. Polzin, B. K. Arbic, S. T. Garner, A. C. Naveira-Garabato, and K. L. Sheen, 2015: Internal Lee Wave Closures: Parameter Sensitivity and Comparison to Observations. *Journal of Geoghysical Research-Oceans*, **120**, 7997–8019.

Venayagamoorthy, S., and O. Fringer, 2006: Numerical simulations of the interaction of internal waves with a shelf-break. *Physics of Fluids*, **18**, 076 603.

Venayagamoorthy, S. K., and J. R. Koseff, 2016: On the flux richardson number in stably stratified turbulence. *Journal of Fluid Mechanics*, **798**, R1.

Wain, D. J., M. C. Gregg, M. H. Alford, R. C. Lien, G. S. Carter, and R. A. Hall, 2013: Propagation and dissipation of the internal tide in upper Monterey Canyon. *J. Geophys. Res.*, **118**, 4855–4877.

WAMDI-Group, 1988: The WAM model-a third generation ocean wave prediction model. *Journal of Physical Oceanography*, **18 (12)**, 1775–1810.

Waterhouse, A. F., J. A. MacKinnon, R. C. Musgrave, S. M. Kelly, A. I. Pickering, and J. Nash, 2017: Internal tide convergence and mixing in a submarine canyon. *Journal of Physical Oceanography*, **47 (2)**, 303–322.

Waterhouse, A. F., and Coauthors, 2014: Global patterns of diapycnal mixing from measurements of the turbulent dissipation rate. *Journal of Physical Oceanography*, **44 (7)**, 1854–1872.

Waterman, S., A. C. Naveira Garabato, and K. L. Polzin, 2013: Internal waves and turbulence in the Antarctic Circumpolar Current. *Journal of Physical Oceanography*, **43**, 259–282.

Waterman, S., K. L. Polzin, A. C. Naveira Garabato, K. L. Sheen, and A. Forryan, 2014: Suppression of internal wave breaking in the Antarctic Circumpolar Current near topography. *Journal of Physical Oceanography*, **44 (5)**, 1466–1492.

Whalen, C. B., 2015: Illuminating spatial and temporal patterns of ocean mixing as inferred from argo profiling floats. Ph.D. thesis, UNIVERSITY OF CALIFORNIA, SAN DIEGO.

Whalen, C. B., J. A. MacKinnon, L. D. Talley, and A. F. Waterhouse, 2015: Estimating the mean diapycnal mixing using a finescale strain parameterization. *Journal of Physical Oceanography*, **45 (4)**, 1174.

Whalen, C. B., L. D. Talley, and J. A. MacKinnon, 2012: Spatial and temporal variability of global ocean mixing inferred from argo profiles. *Geophys. Res. Lett.*, **39 (L18612)**, doi:10.1029/2012GL053 196.

Wijesekera, H. W., L. Padman, T. Dillon, M. Levine, C. Paulson, and R. Pinkel, 1993: The application of internal-wave dissipation models to a region of strong mixing. *Journal of Physical Oceanography*, **23**, 269–286.

Winkel, D. P., M. C. Gregg, and T. B. Sanford, 2002: Patterns of Shear and Turbulence across the Florida Current. *Journal of Physical Oceanography*, **32**, 3269–3285.

Wright, C. J., R. B. Scott, P. Ailliot, and D. Furnival, 2014: Lee wave generation rates in the deep ocean. *Geophysical Research Letters*, **41**, doi:10.1002/2013GL059 087.

Wu, L., Z. Jing, S. Riser, and M. Visbeck, 2011: Seasonal and spatial variations of Southern Ocean diapycnal mixing from Argo profiling floats. *Nature Geoscience*, **4 (6)**, 363–366.

Wunsch, C., 1969: Progressive internal waves on slopes. *Journal of Fluid Mechanics*, **35**, 131–145.

Zhang, L., and H. L. Swinney, 2014: Virtual seafloor reduces internal wave generation by tidal flow. *Phys. Rev. Lett.*, **112**, 14 502.

Zhao, Z., M. H. Alford, J. B. Girton, L. Rainville, and H. L. Simmons, 2016: Global observations of open-ocean mode-1 M_2 internal tides. *Journal of Physical Oceanography*, **46**, 1657–1684, doi:10.1175/JPO-D-15-0105.1.

Zhao, Z., M. H. Alford, J. A. MacKinnon, and R. Pinkel, 2010: Long-range propagation of the semidiurnal internal tide from the Hawaiian Ridge. *Journal of Physical Oceanography*, **40 (4)**, 713–736, doi:10.1175/2009JPO4207.1.

LIST OF FIGURES

Fig. 1. Schematic of internal wave mixing processes in the open ocean that are considered as part of this CPT. Tides interact with topographic features to generate high-mode internal waves (e.g. at mid-ocean ridges) and low-mode internal waves (e.g. at tall steep ridges such as the Hawaiian Ridge). Deep currents flowing over topography can generate lee waves (e.g. in the Southern Ocean). Storms cause inertial oscillations in the mixed layer, which can generate both low and high mode internal waves (e.g. beneath storm tracks). In the open ocean these internal waves can scatter off of rough topography and potentially interact with mesoscale fronts and eddies, until they ultimately dissipate through wave-wave interactions. Internal waves that reach the shelf and slope can scatter, or amplify as propagate towards shallower water. 61

Fig. 2. Depth-averaged diffusivity κ from (a) the upper ocean (from MLD to 1000 m depth) and (b) the full water column, updated from (Waterhouse et al. 2014). The background diffusivity map in (a) comes from the strain-based inferences of diffusivity from Argo floats, updated from (Whalen et al. 2015) with observations included from 2006–2015. (c) Compiled observations of mixing measurements with blue and green squares and diamonds denoting microstructure measurements. Green represents full-depth profiles, while blue denotes microstructure profiles. Purple circles represent inferred diffusivity from a finescale parameterization using LADCP/CTD profiles [dark purple, Kunze et al. (2006); medium purple, Huussen et al. (2012)] and HDSS shipboard shear (light orange). Dark orange circles are diffusivities from density overturns in moored profiles. 62

Fig. 3. a) A snapshot of baroclinic velocity (m/s) from a two-dimensional numerical simulation of internal tides forced by M_2 (semi-diurnal) tidal velocities over rough topography, for parameters corresponding to the Brazil Basin (Nikurashin and Legg 2011); (b) observational time series of internal wave breaking over tall steep topography; here we see northward velocity (upper) and turbulent dissipation rate (lower) oscillate twice a day as the tide flows over Kaena Ridge, Hawaii (Klymak et al. 2008) (c) global energy flux from the M_2 tide into internal tides (in log10 W/m^2) estimated using (top) the topography resolved in the SRTM30_PLUS bathymetry data base and (bottom) a statistical representation of unresolved abyssal hill topography estimates (Melet et al. 2013b); (d) the vertical structure of dissipation from Brazil Basin observations (thick solid curve) and the Polzin 2009 (Eqn. 4) parameterization of nearfield internal tide dissipation (thin solid curve); (e) the impact of the Polzin parameterization in the GFDL CM2G coupled climate model: (top) The Indo-Pacific meridional overturning streamfunction (Sv)(averaged over the final 100 years of a 1000 year simulation) using the Polzin (2009) parameterization, (bottom) the differences in Indo-Pacific meridional overturning streamfunction (Sv) between the simulations with the Polzin (2009) parameterization and the St. Laurent et al. (2002) parameterization as implemented by Simmons et al. (2004b) (from Melet et al. (2013a)). 63

Fig. 4. Farfield internal tide: (a) SSH amplitude (unit: mm) of global mode-1 M_2 internal tides from multisatellite altimetry (Zhao et al. 2016). The light blue color indicates regions of high mesoscale activity, which make extraction of internal tides from altimetry difficult. (b)-(c) Modeled semidiurnal tidal fluxes and comparison to observations: (b) HYCOM modeled semidiurnal internal tide barotropic-to-baroclinic conversion rates (background color) and vertically-integrated energy flux vectors (black arrows, plotted every 768th grid point for clarity), and (c) depth-integrated semidiurnal mode-1 energy fluxes in HYCOM (red arrows) and high-resolution mooring observations to the north of Hawaii (blue arrows) (Ansong et al. 2017). (d)-(f) Impact on thermosteric sea level of using different spatial distribution of remote internal tide energy dissipation in GFDL ESM2G climate model: (d) thermosteric sea level (unit: m) in a reference simulation using a constant background diapycnal diffusivity

for remote internal tide dissipation. Anomalies (in m) of thermosteric sea level from the reference case in (d) for simulations where (e) all internal tide energy is dissipated locally, over the generation site, (f) 20 % of the internal tide energy is dissipated locally and 80 % is dissipated uniformly over the ocean basins with a vertical profile proportional to buoyancy squared N^2 (Melet et al. 2016). 64

Fig. 5. Internal lee waves: a) observations from DIMES showing (left) turbulent dissipation rates (in logarithmic scales from 10^{-10} to 10^{-7} W kg^{-1}) for the Phoenix Ridge (circles in right inset), and (middle) average height above bottom profiles of turbulent kinetic energy dissipation (see details in St. Laurent et al. (2012)), b) power conversion into lee waves (Nikurashin and Ferrari (2011) used in Melet et al. (2014)), c) consequences of parameterized lee wave mixing on the global ocean meridional overturning circulation (Sv, averaged over the final 100 years of 1000 years simulations, from Melet et al. (2014)) , d) global map of depth-integrated dissipation due to parameterized topographic wave drag inserted inline into global 1/25° HYCOM simulation, from Trossman et al. (2016). 65

Fig. 6. Near-inertial internal waves: a) observational example from Alford et al. (2012) showing a 2-year record of wind work (top) and near-inertial kinetic energy (bottom) in the Northeast Pacific; b) one estimate of global power input (shading) and low-mode NIW energy fluxes (arrows; Simmons and Alford (2012)). c) Impact of near-inertial waves on annual mean precipitation in ocean climate models. The upper panel shows the mean precipitation (mm/day) from an experiment where the NI flux is set to 0.34 TW and the lower panel shows the same experiment but with a doubling of the NI flux to 0.68 TW. The total tropical precipitation in the two experiments differs by less than 1% An increase in near-inertial energy flux within observational uncertainties ameliorates the double ITCZs in the Atlantic and Pacific, and creates the South Pacific Convergence Zone; three significant improvements for climate simulations of tropical precipitation. 66

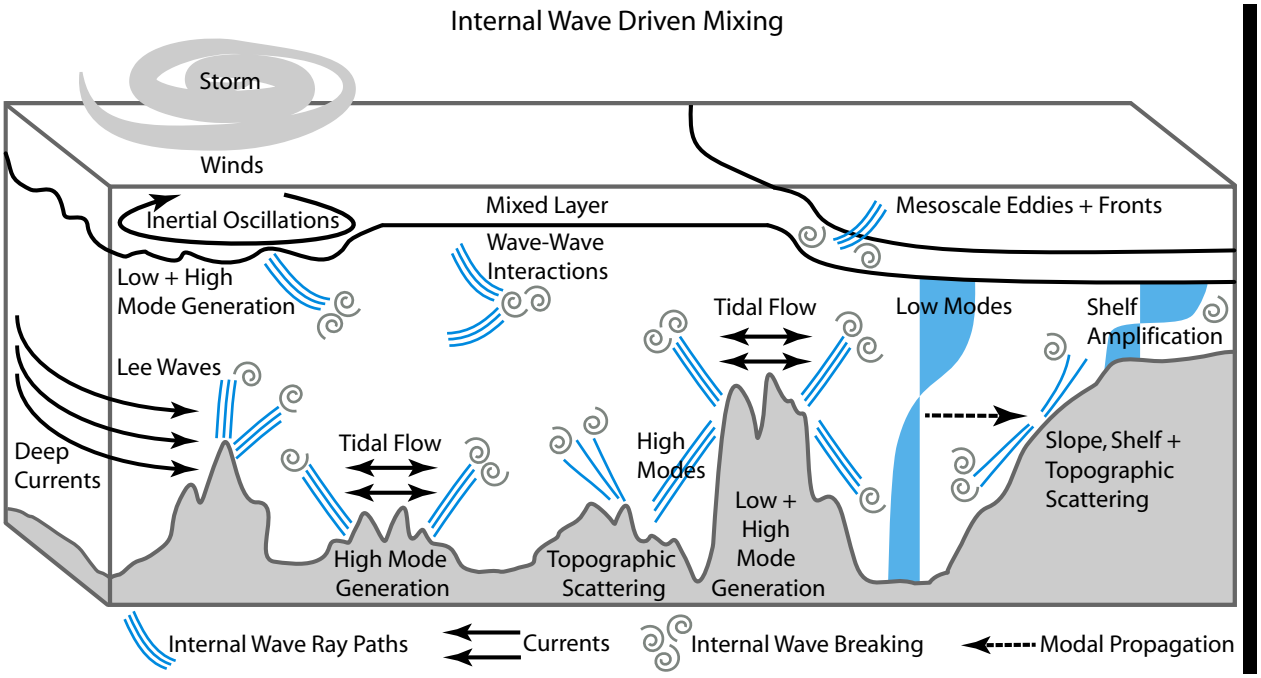

FIG. 1. Schematic of internal wave mixing processes in the open ocean that are considered as part of this CPT. Tides interact with topographic features to generate high-mode internal waves (e.g. at mid-ocean ridges) and low-mode internal waves (e.g. at tall steep ridges such as the Hawaiian Ridge). Deep currents flowing over topography can generate lee waves (e.g. in the Southern Ocean). Storms cause inertial oscillations in the mixed layer, which can generate both low and high mode internal waves (e.g. beneath storm tracks). In the open ocean these internal waves can scatter off of rough topography and potentially interact with mesoscale fronts and eddies, until they ultimately dissipate through wave-wave interactions. Internal waves that reach the shelf and slope can scatter, or amplify as propagate towards shallower water.

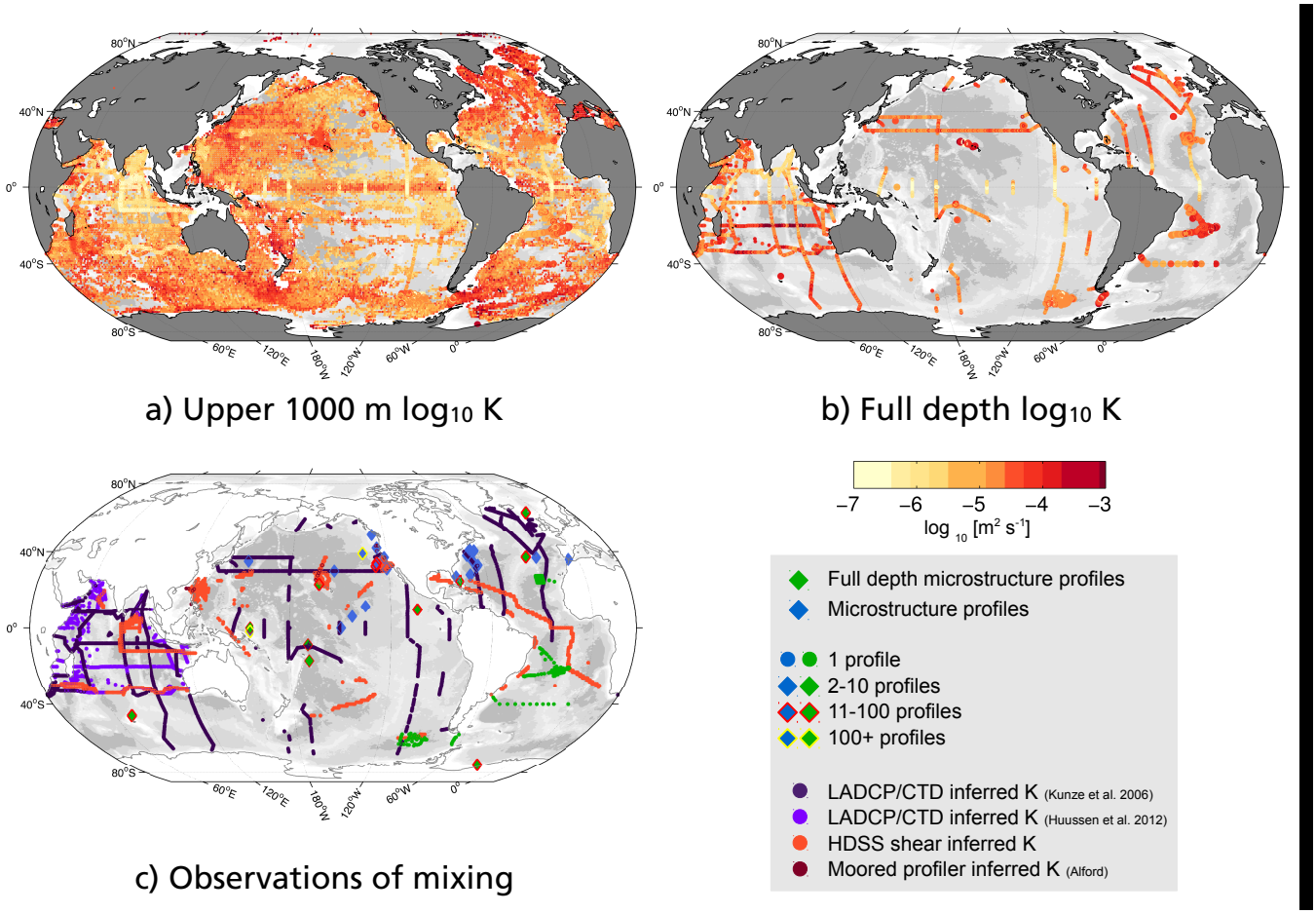

FIG. 2. Depth-averaged diffusivity κ from (a) the upper ocean (from MLD to 1000 m depth) and (b) the full water column, updated from (Waterhouse et al. 2014). The background diffusivity map in (a) comes from the strain-based inferences of diffusivity from Argo floats, updated from (Whalen et al. 2015) with observations included from 2006–2015. (c) Compiled observations of mixing measurements with blue and green squares and diamonds denoting microstructure measurements. Green represents full-depth profiles, while blue denotes microstructure profiles. Purple circles represent inferred diffusivity from a finescale parameterization using LADCP/CTD profiles [dark purple, Kunze et al. (2006); medium purple, Huussen et al. (2012)] and HDSS shipboard shear (light orange). Dark orange circles are diffusivities from density overturns in moored profiles.

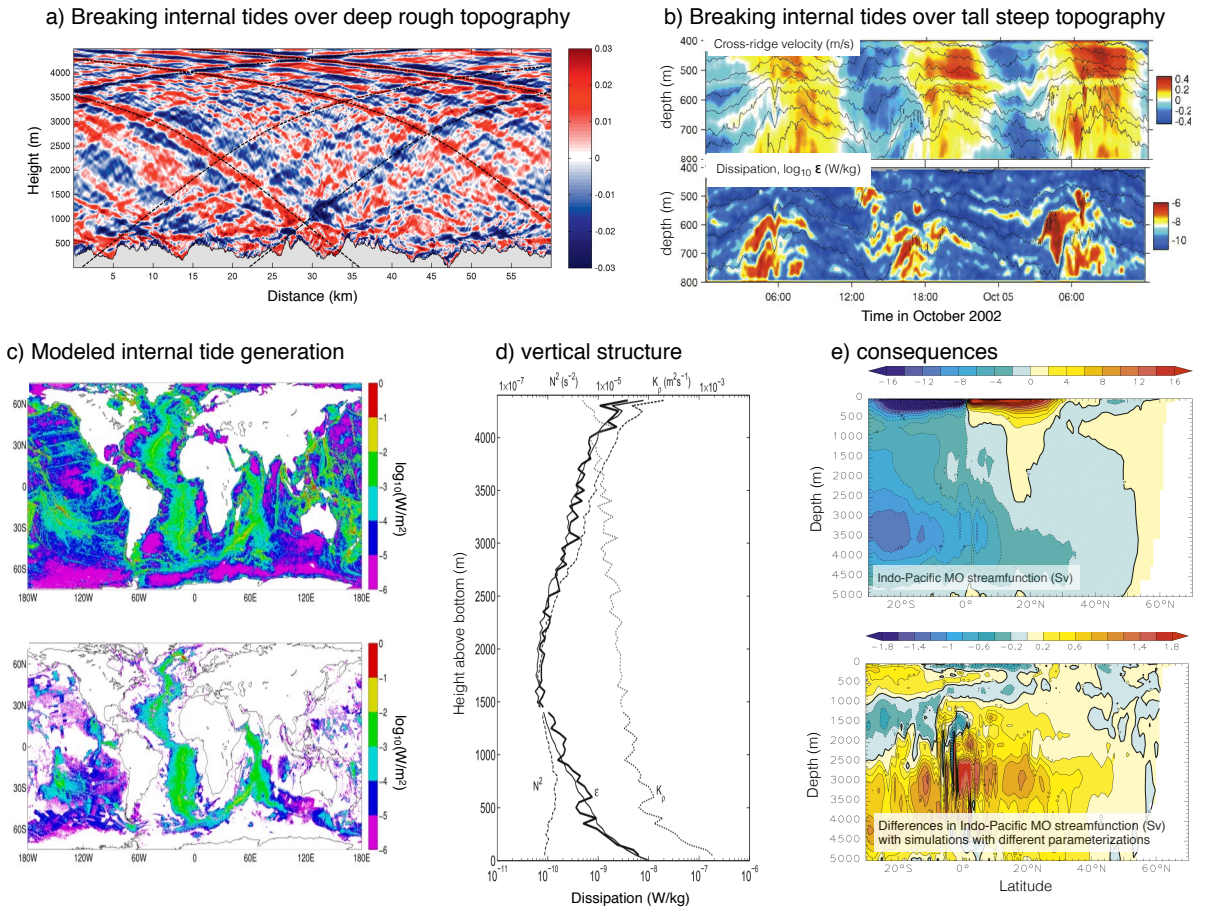

FIG. 3. a) A snapshot of baroclinic velocity (m/s) from a two-dimensional numerical simulation of internal tides forced by M_2 (semi-diurnal) tidal velocities over rough topography, for parameters corresponding to the Brazil Basin (Nikurashin and Legg 2011); (b) observational time series of internal wave breaking over tall steep topography; here we see northward velocity (upper) and turbulent dissipation rate (lower) oscillate twice a day as the tide flows over Kaena Ridge, Hawaii (Klymak et al. 2008) (c) global energy flux from the M_2 tide into internal tides (in log10 W/m^2) estimated using (top) the topography resolved in the SRTM30_PLUS bathymetry data base and (bottom) a statistical representation of unresolved abyssal hill topography estimates (Melet et al. 2013b); (d) the vertical structure of dissipation from Brazil Basin observations (thick solid curve) and the Polzin 2009 (Eqn. 4) parameterization of nearfield internal tide dissipation (thin solid curve); (e) the impact of the Polzin parameterization in the GFDL CM2G coupled climate model: (top) The Indo-Pacific meridional overturning streamfunction (Sv)(averaged over the final 100 years of a 1000 year simulation) using the Polzin (2009) parameterization, (bottom) the differences in Indo-Pacific meridional overturning streamfunction (Sv) between the simulations with the Polzin (2009) parameterization and the St. Laurent et al. (2002) parameterization as implemented by Simmons et al. (2004b) (from Melet et al. (2013a)).

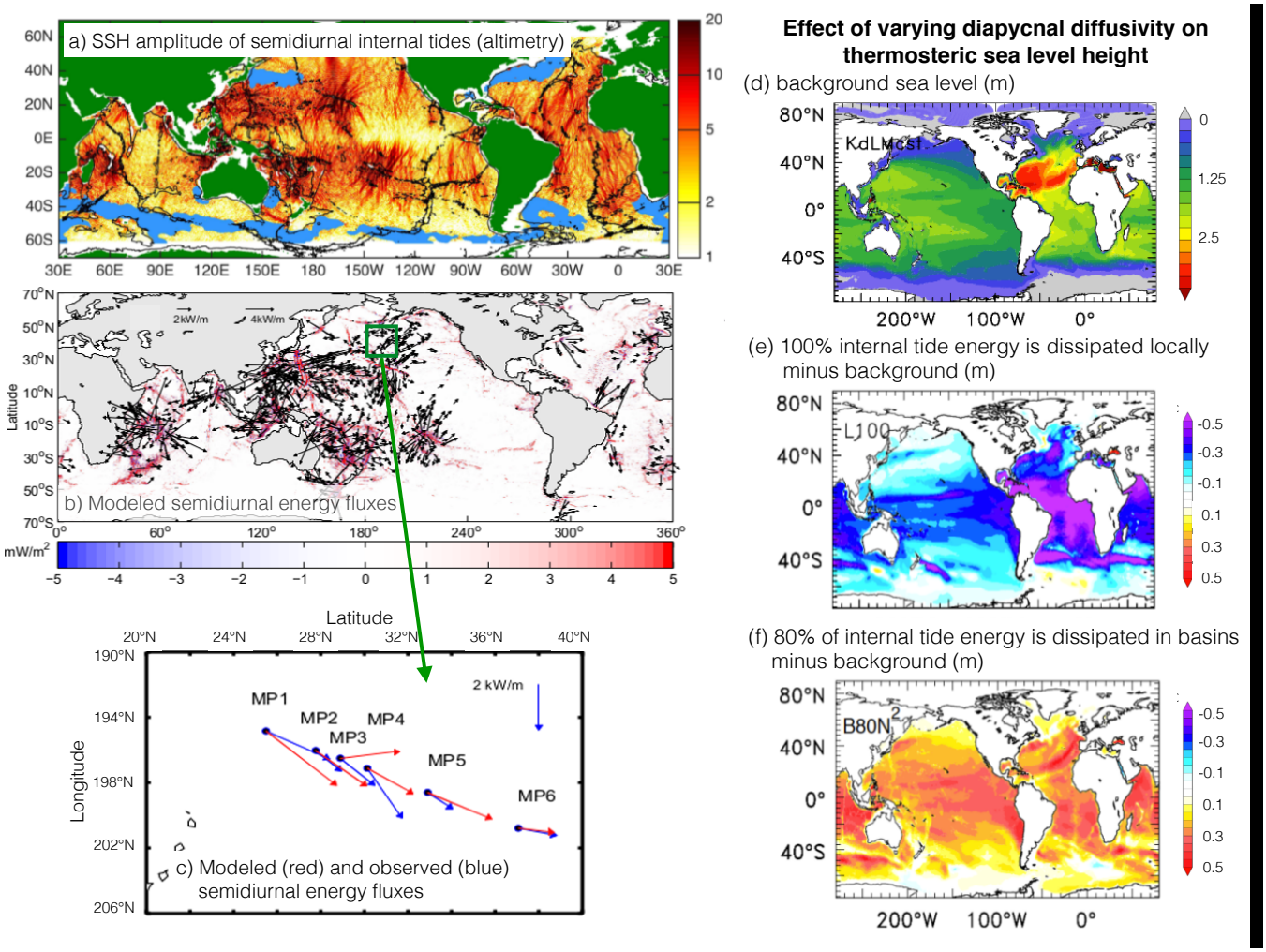

FIG. 4. Farfield internal tide: (a) SSH amplitude (unit: mm) of global mode-1 M_2 internal tides from multisatellite altimetry (Zhao et al. 2016). The light blue color indicates regions of high mesoscale activity, which make extraction of internal tides from altimetry difficult. (b)-(c) Modeled semidiurnal tidal fluxes and comparison to observations: (b) HYCOM modeled semidiurnal internal tide barotropic-to-baroclinic conversion rates (background color) and vertically-integrated energy flux vectors (black arrows, plotted every 768th grid point for clarity), and (c) depth-integrated semidiurnal mode-1 energy fluxes in HYCOM (red arrows) and high-resolution mooring observations to the north of Hawaii (blue arrows) (Ansong et al. 2017). (d)-(f) Impact on thermosteric sea level of using different spatial distribution of remote internal tide energy dissipation in GFDL ESM2G climate model: (d) thermosteric sea level (unit: m) in a reference simulation using a constant background diapycnal diffusivity for remote internal tide dissipation. Anomalies (in m) of thermosteric sea level from the reference case in (d) for simulations where (e) all internal tide energy is dissipated locally, over the generation site, (f) 20 % of the internal tide energy is dissipated locally and 80 % is dissipated uniformly over the ocean basins with a vertical profile proportional to buoyancy squared N^2 (Melet et al. 2016).

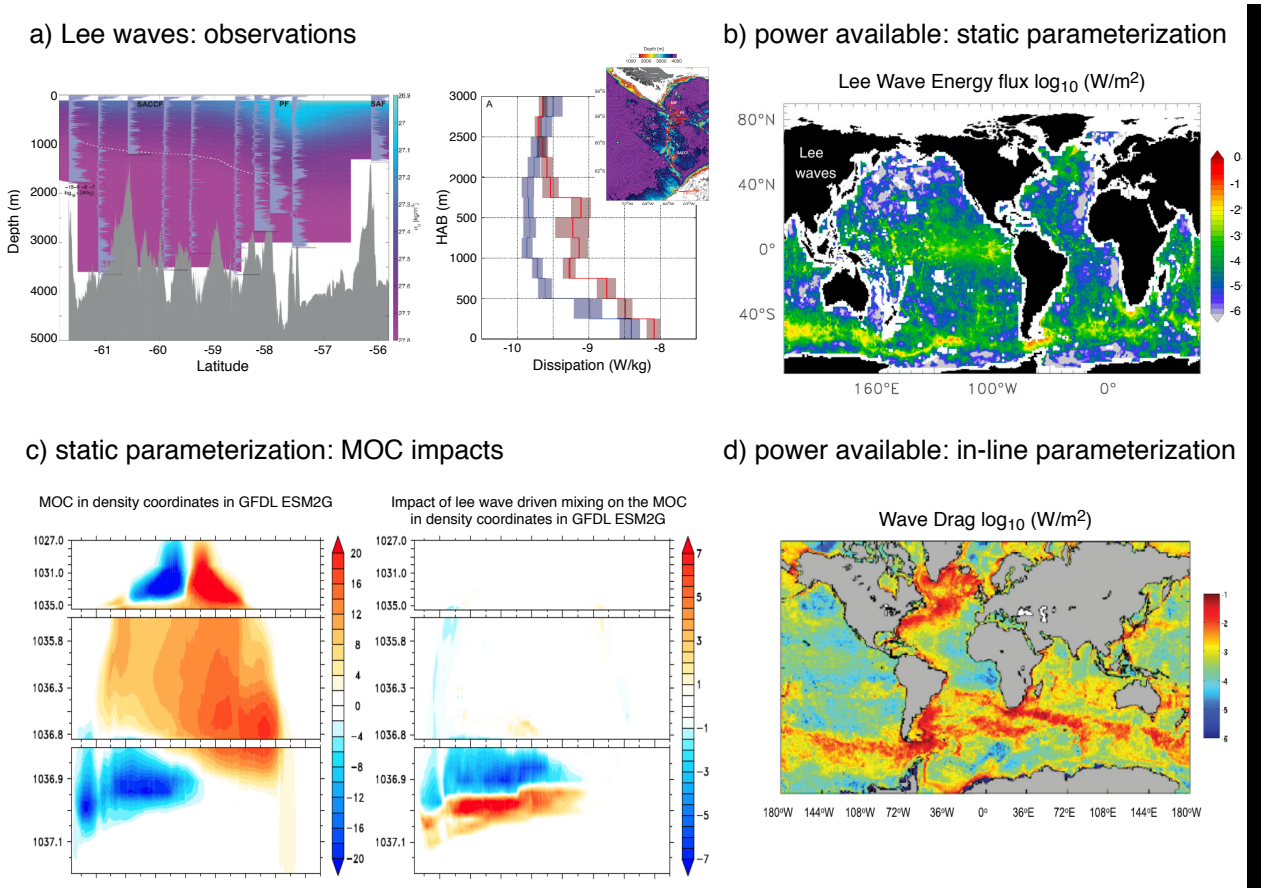

FIG. 5. Internal lee waves: a) observations from DIMES showing (left) turbulent dissipation rates (in logarithmic scales from 10^{-10} to 10^{-7} W kg^{-1}) for the Phoenix Ridge (circles in right inset), and (middle) average height above bottom profiles of turbulent kinetic energy dissipation (see details in St. Laurent et al. (2012)), b) power conversion into lee waves (Nikurashin and Ferrari (2011) used in Melet et al. (2014)), c) consequences of parameterized lee wave mixing on the global ocean meridional overturning circulation (Sv, averaged over the final 100 years of 1000 years simulations, from Melet et al. (2014)) , d) global map of depth-integrated dissipation due to parameterized topographic wave drag inserted inline into global 1/25° HYCOM simulation, from Trossman et al. (2016).

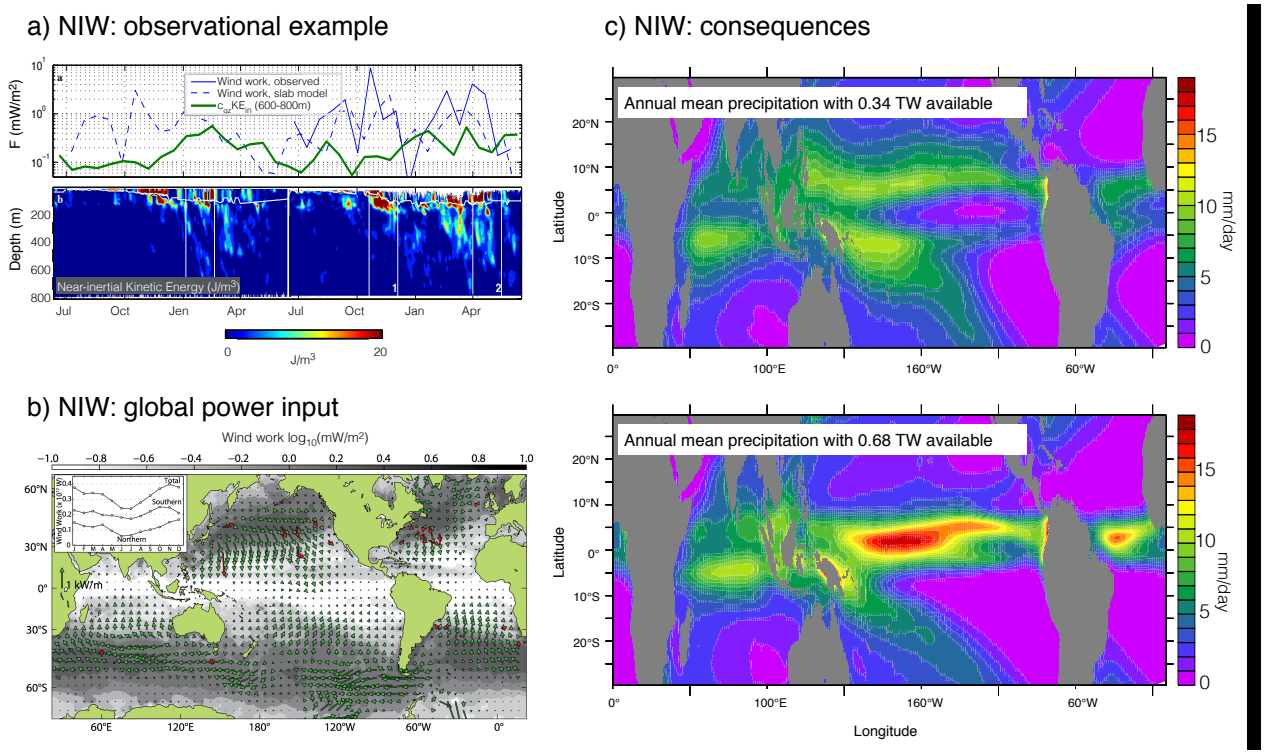

FIG. 6. Near-inertial internal waves: a) observational example from Alford et al. (2012) showing a 2-year record of wind work (top) and near-inertial kinetic energy (bottom) in the Northeast Pacific; b) one estimate of global power input (shading) and low-mode NIW energy fluxes (arrows; Simmons and Alford (2012)). c) Impact of near-inertial waves on annual mean precipitation in ocean climate models. The upper panel shows the mean precipitation (mm/day) from an experiment where the NI flux is set to 0.34 TW and the lower panel shows the same experiment but with a doubling of the NI flux to 0.68 TW. The total tropical precipitation in the two experiments differs by less than 1% An increase in near-inertial energy flux within observational uncertainties ameliorates the double ITCZs in the Atlantic and Pacific, and creates the South Pacific Convergence Zone; three significant improvements for climate simulations of tropical precipitation.